Remapping-free variational h-adaption for strongly coupled thermo-mechanical problems

Rohit Pethe, Thomas Heuzé, Laurent Stainier

Remapping-free variational h-adaption for strongly coupled thermo-mechanical problems

Rohit Pethe[a], Thomas Heuzé[a,*], Laurent Stainier[a]

[a]*Research Institute in Civil and Mechanical Engineering (GeM, UMR 6183 CNRS)*
École Centrale de Nantes, 1 rue de la Noë, F-44321 Nantes, France

Abstract

A mesh adaption approach for strongly coupled problems is proposed, based on a variational principle. The adaption technique relies on optimality properties of an energy-like potential and is hence free from error estimates and the associated computational cost. According to the saddle point nature of this variational principle, a staggered solution approach appears more natural and leads to separate the mesh adaption for the mechanical and the thermal fields. Using different meshes for different phenomena, precise solutions for the various fields under consideration are obtained. Mesh adaption steps (subdivision, merging) are local operations only, so that no complex remapping procedures are necessary to transfer internal variables. In practice, nearest-neighbor interpolations were used. The proposed method is shown to be cost effective with respect to a uniform mesh refinement. Some applications of the proposed approach are presented on various examples, including shear banding and friction welding.

Keywords: Variational mesh adaption, Thermo-mechanics, Coupled problem, Rivara's LEPP algorithm, Single edge bisection technique

1. Introduction

Several industrial phenomena involve strongly coupled problems, for example, forging, machining, friction welding and many others. In these problems, the dynamic and transient effects cause the domains of interest to change rapidly. In the framework of the finite element method, this means that the domains of interest change their spatial location with time. Therefore, in order to obtain precise solutions at each time step, a mesh adaption strategy is required.

Mesh adaption processes can be divided into three broad categories. The first one is the h-adaption, where the mesh size is optimized [21]. It may contain processes of element refinement and/or coarsening. This approach is considered in this article. Second, r-adaption keeps the same number of nodes, changes their location and the connectivity [56]. Third, p-adaption adapts the order of the interpolation polynomial within elements [54]. Mesh adaption strategies depend on both the adaptive techniques and adaption criteria. Adaptive techniques essentially deal with geometrical aspects of adaption, whereas the adaption criteria captures the peculiarity of the problem under consideration.

Several mesh adaption techniques were proposed in the literature. Rivara et al. [60, 59, 58] proposed explicit updates for local mesh changes. Molinari et al. [49] used a local coarsening and refinement method based on the mesh size for shear bands. Mesh adaption for shear bands has also been studied in plane strain [6, 10]. Global mesh adaption procedures create a completely new mesh and use remapping procedures to transfer internal variables [52, 57]. Using gradient based indicators, the global remeshing technique has been applied to impact problems [22]. Global remeshing techniques also handle mesh distortions in machining problems [46]. Methods based on global remeshing of the domain of interest require to transfer internal variables between meshes, which can lead to artificial diffusion of the latter unless specific methods are used [11]. Camacho et al. [13] proposed remeshing methods using

*Corresponding author
Email address: thomas.heuze@ec-nantes.fr (Thomas Heuzé)

advancing front methods for ballistic penetration problems. Mesh adaption was also used in [19, 68] for the shape optimization of structures. Grinspun et al. [27] proposed the CHARMS method for hierarchical mesh refinement.

Classically, mesh adaption criteria have been based on error-estimates or mesh skewness. The commonly used Z^2 error estimate proposed by Zienkiewicz and Zhu [72] uses stresses within an element and is based on a recovery process to obtain the reference nodal stresses. The difference between the element and the reference stresses provides a gradient based error estimate. Curvature based error estimates have been proposed by Borouchaki et al. [10]. Error estimates based on the error in constitutive relation have also been studied [39, 17, 38]. In these methods, the finite element solution is described as a displacement-stress pair such that the displacements satisfy kinematic constraints like boundary conditions and initial conditions while the stresses satisfy the equilibrium conditions. The displacements and the stresses do not satisfy the constitutive relations (stress-strain relations) which provides a measure of the error, which they refer to as the constitutive relation error. Romero et al. [62] proposed an error estimate based on the time update. Gurtin [28] used configurational forces for r-adaption. Some authors also used gradients of physical quantities as mesh adaption criteria [6, 10, 52]. Error estimates can also be based on variational principles [33, 34, 14, 57]. Many other error estimators were studied by various researchers [2, 36, 43, 26].

While mesh adaption using error estimation is well established for single field problems, only few attempts have been made towards mesh adaption methods for strongly coupled problems. Most of the methods available in the literature adapt the mesh for only one of the considered fields [4]. Solin et al. [63] used a multimesh adaption approach for weakly coupled problems, but the method is limited to thermo-elasticity. Vokas et al. [69] consider a single mesh and h-refinement affects all fields simultaneously, therefore the method fails to capture different scales and spatial resolutions of different fields. Moreover, the mesh adaption criteria relies on error estimators that work well with linear constitutive models, but are very complex in the case of non-linear constitutive models due to their need to reconstruct admissible fields. Therefore, it can appear difficult and expensive to use this approach for strongly coupled problems with non-linear constitutive models and/or large deformation.

In the present article, we present a strategy of mesh adaption for thermomechanical strongly coupled problems based on the variational approach of [53]. The variational form of the coupled thermo-elastic and thermo-visco-elastic problems has been extensively investigated [9, 8, 5, 7, 31, 48]. Variational principles for equilibrium problems of general dissipative solids in the isothermal setting have been proposed in [15, 18, 29, 30, 45]. Next, variational visco-plastic constitutive updates were introduced by Stainier and Ortiz [53]. Variational formulations have also been proposed for the case of brittle and ductile damage in [3, 24, 37]. Formulations for coupled thermo-mechanical problems involving non-linear dissipative behaviour, such as thermo-elasto-visco-plasticity have been more recently summarized by Stainier [65, 70]. In this paper, we focus on initial boundary value problems that gather transient heat transfer and a quasi-static mechanical problem.

The adaption strategy for coupled problems is derived from a method proposed for purely structural problems by Mosler et al. [50, 51]. This variational h-adaption method has also recently been applied to phase field approach to model fracture [44]. The proposed mesh adaption criteria depends on the error indicated by the variational functional [70, 65]. The method is free from any costly error estimation, and the variational functional itself drives the mesh refinement and coarsening. The approach relies on a staggered approach [1] and uses different meshes for different fields. The sequential adaption of different meshes allows to capture different scales and spatial resolutions of the different fields. Assuming a constant distribution of internal variables over elementary cells consisting of the intersection between Voronoï cells and triangular elements, complex remapping procedures causing significant numerical diffusion from the initial mesh to the adapted mesh can be avoided. The same holds true between the steps of the staggered scheme.

Two mesh adaption techniques are presented in this work. First, a single edge bisection technique [50], allowing the generation of anisotropic meshes. Second, Rivara's LEPP algorithm [60] is used which constrains the element aspect ratio. The mesh adaption criterion is based on an error indicator provided by the variational functional. The authors earlier proposed a strategy of using this error indicator for 1D thermal and thermo-mechanical problems [55]. However, the extension of the strategy to 2D and 3D problems poses additional difficulties. These difficulties are addressed in this article. In addition to being free from error estimates and remapping procedures, the algorithm also proves to be cost effective with respect to using uniform refinement technique.

The structure of the article is as follows: in Section 2, the continuous and discrete thermo-mechanical variational formulations are reviewed, the latter being formulated as an incremental boundary value problem. Examples of practical expressions for the variational functionals are given for some particular media of interest (thermoelasticity,

thermo-elastic-viscoplasticity). In Section 3, the mesh adaption algorithm is explained. The local error indicators based on the variational functional are presented. Finally, Section 4 shows some numerical examples. First, a steady state thermal problem with an existing analytical solution is examined for error analysis purpose. Then, test cases involving a linear thermo-elastic medium and shear banding are presented. Finally, a test case representative of linear friction welding is simulated.

2. Variational formulation of the thermo-mechanical initial boundary value problem

2.1. Continuum setting

The variational formulation of the thermo-mechanical initial boundary value problem introduced in [70] consists of a functional admitting a saddle point involving internal variables $\mathbf{Z}$ and external fields, the displacement $\mathbf{u}$ and the temperature T. Since the optimality of the functional with respect to internal variables involves local quantities defined at the scale of a material point, while its optimality with respect to external fields involve quantities defined on the whole domain Ω, both are described separately hereafter.

2.1.1. Local constitutive problem

The set of constitutive equations for a nonlinear dissipative model can admit a variational principle by defining the functional $D(\dot{\mathbf{F}}, \dot{\eta}, \dot{\mathbf{Z}}, T; \mathbf{F}, \eta, \mathbf{Z})$:

$$D(\dot{\mathbf{F}}, \dot{\eta}, \dot{\mathbf{Z}}, T; \mathbf{F}, \eta, \mathbf{Z}) = \frac{d}{dt}[U(\mathbf{F}, \eta, \mathbf{Z})] - \rho_0 \dot{\eta} T + \Phi\left(\dot{\mathbf{F}}, \dot{\mathbf{Z}}; \mathbf{F}, \Theta(\mathbf{F}, \eta, \mathbf{Z}), \mathbf{Z}\right) \tag{1}$$

where $\mathbf{F}$ is the deformation gradient, ρ_0 is the initial mass density, η is the entropy, U is the internal energy density, Φ is the convex dissipation potential and Θ denotes some equilibrium or internal temperature given by:

$$\Theta(\mathbf{F}, \eta, \mathbf{Z}) = \frac{1}{\rho_0} \frac{\partial U}{\partial \eta}(\mathbf{F}, \eta, \mathbf{Z}) \tag{2}$$

One can rewrite the above equation in terms of Helmholtz's free energy $W(\mathbf{F}, T, \mathbf{Z})$ as follows:

$$D(\dot{\mathbf{F}}, \dot{\eta}, \dot{\mathbf{Z}}, T; \mathbf{F}, \eta, \mathbf{Z}) = \frac{d}{dt}[W(\mathbf{F}, T, \mathbf{Z})] + \rho_0 \eta \dot{T} + \Phi\left(\dot{\mathbf{F}}, \dot{\mathbf{Z}}; \mathbf{F}, \Theta(\mathbf{F}, \eta, \mathbf{Z}), \mathbf{Z}\right) \tag{3}$$

Thermodynamic forces consist of the first Piola-Kirchhoff stress tensor $\mathbf{P}$ conjugate to the deformation gradient $\mathbf{F}$, and of forces $\mathbf{Y}$ conjugate to internal variables $\mathbf{Z}$. These thermodynamic forces can be additively decomposed into reversible and irreversible components [71]:

$$\begin{aligned} \mathbf{P} &= \mathbf{P}^{\text{rev}} + \mathbf{P}^{\text{irr}} \\ \mathbf{Y} &= \mathbf{Y}^{\text{rev}} + \mathbf{Y}^{\text{irr}} \end{aligned} \tag{4}$$

such that their reversible components are conjugate to state variables $(\mathbf{F}, \mathbf{Z})$ through Helmholtz's free energy:

$$\begin{aligned} \mathbf{P}^{\text{rev}} &= \frac{\partial W}{\partial \mathbf{F}} \\ \mathbf{Y}^{\text{rev}} &= \frac{\partial W}{\partial \mathbf{Z}} \end{aligned} \tag{5}$$

Since internal variables should not produce any work, *i.e.* $\mathbf{Y} \cdot \dot{\mathbf{Z}} = 0$, $\forall \dot{\mathbf{Z}}$, it follows that

$$\mathbf{Y}^{\text{rev}} + \mathbf{Y}^{\text{irr}} = 0. \tag{6}$$

The reversible power per unit volume received by the system $\dot{w}_\tau$ can be defined as

$$\dot{w}_\tau = \frac{d}{dt}[U(\mathbf{F}, \eta, \mathbf{Z})] - \rho_0 \dot{\eta} T = \frac{d}{dt}[W(\mathbf{F}, T, \mathbf{Z})] + \rho_0 \eta \dot{T} = \mathbf{P}^{\text{rev}} \cdot \dot{\mathbf{F}} + \mathbf{Y}^{\text{rev}} \cdot \dot{\mathbf{Z}} = (\mathbf{P} - \mathbf{P}^{\text{irr}}) \cdot \dot{\mathbf{F}} - \mathbf{Y}^{\text{irr}} \cdot \dot{\mathbf{Z}} \tag{7}$$

whereas the dissipation potential represents the power per unit volume that can be dissipated. Therefore, the functional D can be interpreted as the sum of the two homogeneous terms representing a power per unit volume. One is associated to reversible processes, the other is associated with irreversible processes.

The general thermo-mechanical rate problem does not have an obvious variational structure. The weak formulation obtained by multiplying the field equations by admissible variation of fields does not derive from a potential. It was shown in [70] that using two key ideas, the thermo-mechanical initial boundary value problem can be made symmetric. First, a two-field thermal formulation allows to separate some internal temperature Θ from the unknown external temperature T appearing in the energy equation. Equality between these two temperatures $\Theta = T$ is enforced as an internal constraint in the model, and relaxed in state laws. Second, in order to find a variational form to the general rate problem, an integration factor that allows to recover the requisite symmetry of the strong form is identified. Yang et al. [70] identifies the integrating factor $\frac{T}{\Theta}$ by considering a time re-scaling of rate quantities appearing as arguments of the dissipation potential, which thus reads $\Phi\left(\frac{T}{\Theta}\dot{\mathbf{F}}, \frac{T}{\Theta}\dot{\mathbf{Z}}; \mathbf{F}, T, \mathbf{Z}\right)$.

A multifield variational principle is then defined. Given an external state $\{\mathbf{u}, T\}$, the stationarity of the functional D with respect to the rate of internal variables

$$D_{\text{eff}} = \inf_{\dot{\mathbf{z}}} D = \inf_{\dot{\mathbf{z}}} \left\{ \frac{dU}{dt} - \rho\dot{\eta}T + \Phi\left(\frac{T}{\Theta}\dot{\mathbf{F}}, \frac{T}{\Theta}\dot{\mathbf{Z}}; \mathbf{F}, \Theta(\mathbf{F}, \eta, \mathbf{Z}), \mathbf{Z}\right) \right\} \tag{8}$$

yields the effective value D_{eff} of the functional D thanks to the convexity of the dissipation potential, from which the evolutions laws read

$$\mathbf{Y}^{\text{irr}} = \frac{T}{\Theta}\frac{\partial \Phi}{\partial \dot{\mathbf{Z}}} = -\frac{\partial W}{\partial \mathbf{Z}}, \tag{9}$$

where the second equality results from (6). The Piola-Kirchchoff stress tensor $\mathbf{P}$ is obtained by the variation of D_{eff} with respect to $\dot{\mathbf{F}}$:

$$\frac{\partial D_{\text{eff}}}{\partial \dot{\mathbf{F}}} = \frac{\partial W}{\partial \mathbf{F}} + \frac{T}{\Theta}\frac{\partial \Phi}{\partial \dot{\mathbf{F}}} = \mathbf{P}^{\text{rev}} + \mathbf{P}^{\text{irr}} = \mathbf{P} \tag{10}$$

Equality between the equilibrium and the external temperatures is recovered through the optimality of D with respect to the entropy rate

$$\operatorname*{stat}_{\dot{\eta}} D(\dot{\mathbf{F}}, \dot{\eta}, \dot{\mathbf{Z}}, T; \mathbf{F}, \eta, \mathbf{Z}) \Leftrightarrow \frac{\partial U}{\partial \eta} - \rho_0 T = 0 \Leftrightarrow T = \Theta(\mathbf{F}, T, \mathbf{Z}) \tag{11}$$

The variation of D_{eff} with respect to the external temperature T gives

$$\frac{\partial D_{\text{eff}}}{\partial T} = -\rho_0\dot{\eta} + \frac{\mathcal{D}_{int}}{T}, \tag{12}$$

where $\mathcal{D}_{int}$ denotes the mechanical dissipation caused by the dissipative forces $\mathbf{P}^{\text{irr}}$ and $\mathbf{Y}^{\text{irr}}$

$$\mathcal{D}_{int} = \mathbf{P}^{\text{irr}} : \dot{\mathbf{F}} + \mathbf{Y}^{\text{irr}} \cdot \dot{\mathbf{Z}} \geq 0 \tag{13}$$

that should be non-negative.

2.1.2. Initial boundary value problem

The initial boundary value problem consists of the transient heat transfer problem plus a quasi-static mechanical one defined in the initial domain Ω_0 (at time $t = 0$), whose solution consists of the displacement field $\mathbf{u}$, the temperature field T and internal variables $\mathbf{Z}$. The latter being determined locally, the external fields $\{\mathbf{u}, T\}$ are to be determined in the domain Ω_0. Assuming a non-overlapping partition of Dirichlet and Neumann subparts of the boundary $\partial\Omega_0$ of the domain Ω_0 for both thermal and mechanical physics, boundary conditions are prescribed such that $\mathbf{u} = \bar{\mathbf{u}}$ on $\partial_u\Omega_0$, $\mathbf{P} \cdot \mathbf{N} = \bar{\mathbf{t}}$ on $\partial_t\Omega_0$, $T = \bar{T}$ on $\partial_T\Omega_0$ and $\mathbf{Q} \cdot \mathbf{N} = \bar{Q}$ on $\partial_Q\Omega_0$, where $\bar{\mathbf{u}}$, $\bar{\mathbf{t}}$, $\bar{T}$ and $\bar{Q}$ are the imposed displacement, tractions, temperature and outward heat flux density respectively. Besides, $\mathbf{P}$ denotes the first Piola-Kirchhoff stress tensor, $\mathbf{Q}$ the outward heat flux density, and $\mathbf{N}$ the outward unit normal to the initial boundary $\partial\Omega_0$. As shown by Yang

et al. [70], the variational functional for this initial boundary value problem is given by:

$$\Phi(\dot{\mathbf{u}},\dot{\eta},T)=\int_{\Omega_0}\left[D_{\text{eff}}(\dot{\mathbf{F}},\dot{\eta},T)-\chi\left(-\frac{\boldsymbol{\nabla}T}{T};\mathbf{F},\Theta(\mathbf{F},\eta,\mathbf{Z}),\mathbf{Z}\right)\right]dV \\ +\int_{\Omega_0}\left[\rho r\log\frac{T}{\Theta}-\rho_0\mathbf{b}\cdot\dot{\mathbf{u}}\right]dV-\int_{\partial_t\Omega_0}\bar{\mathbf{t}}\cdot\dot{\mathbf{u}}da-\int_{\partial_Q\Omega_0}\bar{Q}\log\frac{T}{\Theta}da \quad (14)$$

where r and $\mathbf{b}$ refer to the distributed heat source and body force densities, both per unit mass; dV and da refer to infinitesimal elements of volume and area respectively. Following Biot [9], the heat conduction potential χ is given as follows:

$$\chi=\frac{1}{2T}\boldsymbol{\nabla}T\cdot\mathbf{K}\cdot\boldsymbol{\nabla}T \quad (15)$$

where $\mathbf{K}$ is the thermal conductivity tensor. Stationarity of Φ with respect to $\dot{\mathbf{u}}$ yields the weak form of the linear momentum balance

$$<D_{\dot{\mathbf{u}}}\Phi,\delta\dot{\mathbf{u}}>=-\int_{\Omega_0}\delta\dot{\mathbf{u}}\cdot\{\boldsymbol{\nabla}_0\mathbf{P}+\rho\mathbf{b}\}\,dV-\int_{\partial_t\Omega_0}\delta\dot{\mathbf{u}}\cdot(\bar{\mathbf{t}}-\mathbf{P}\cdot\mathbf{n})\,da=0, \quad (16)$$

while its stationarity with respect to T yields the weak work of the energy balance

$$<D_T\Phi,\delta T>=\int_{\Omega_0}\delta T\left\{-\rho_0\dot{\eta}+\frac{\mathcal{D}_{int}}{T}\right\}dV+\int_{\Omega_0}\Theta\boldsymbol{\nabla}\left(\frac{\delta T}{T}\right)\cdot\mathbf{K}\cdot\frac{\boldsymbol{\nabla}T}{T}dV \\ +\int_{\Omega_0}\frac{\rho r\delta T}{\Theta}dV-\int_{\partial_Q\Omega_0}\frac{\bar{Q}\delta T}{\Theta}da=0. \quad (17)$$

Finally, its optimality with respect to $\dot{\eta}$ yields (11). Hence, the extremal point of the functional Φ is expressed as

$$\{\dot{\mathbf{u}},\dot{\eta},T\}=\arg\operatorname*{stat}_{\dot{\mathbf{u}}}\inf_{\dot{\eta}}\sup_{T}\Phi(\dot{\mathbf{u}},\dot{\eta},T) \quad (18)$$

However, in a number of cases, depending on the actual expression for D_{eff}, the extremal point will actually correspond to a saddle-point, so that the optimality with respect to $\dot{\mathbf{u}}$ defines a minimum.

2.2. Discrete setting

2.2.1. Local time-discrete constitutive problem

Consider the discrete time increment $\Delta t=t-t_0$, and assume the local material state $\{\mathbf{F}_0,\eta_0,\mathbf{Z}_0\}$ is completely known at time t_0. In order to compute internal variables $\mathbf{Z}$, an incremental function $\mathscr{I}(\mathbf{F},T,\mathbf{Z})$ is sought in such a way that it approximates the integral of the functional D (1) over the time increment Δt:

$$\mathscr{I}(\mathbf{F},T,\mathbf{Z};\mathbf{F}_0,T_0,\mathbf{Z}_0)\approx\int_{t_0}^{t}D(\dot{\mathbf{F}},\dot{\eta},\dot{\mathbf{Z}},T(\tau);\mathbf{F}(\tau),\eta(\tau),\mathbf{Z}(\tau))d\tau \\ =W(\mathbf{F},T,\mathbf{Z})-W_0+\rho_0\eta_0\Delta T+\Delta t\left\langle\Phi\left(\frac{T}{T_0}\frac{\Delta\mathbf{F}}{\Delta t},\frac{T}{T_0}\frac{\Delta\mathbf{Z}}{\Delta t};\mathbf{F}(\tau),T(\tau),\mathbf{Z}(\tau)\right)\right\rangle \quad (19)$$

where the identity $\dot{U}-\rho_0\dot{\eta}T=\dot{W}+\rho_0\eta\dot{T}$ has been used. In the above equation, the definitions $\Delta(\cdot)=(\cdot)-(\cdot)_0$, $W_0=W(\mathbf{F}_0,T_0,\mathbf{Z}_0)$ have been used, and the factor $\frac{T}{\Theta}$ have been replaced by $\frac{T}{T_0}$ where T_0 denotes the temperature at time t_0. This corresponds to the time discretization of the local functional (1) associated with the local variational principle, as shown in [70]. The brackets $\langle\bullet\rangle$ denotes a consistent average value of the quantity $(\bullet)$ over the time increment. More details are provided on its computation in [64, 12]. The incremental variational update for internal variables $\mathbf{Z}$ takes the form of the following minimization problem:

$$\mathcal{W}(\mathbf{F},T;\mathbf{F}_0,T_0,\mathbf{Z}_0)=\inf_{\mathbf{Z}}\mathscr{I}(\mathbf{F},T,\mathbf{Z};\mathbf{F}_0,T_0,\mathbf{Z}_0), \quad (20)$$

that is

$$\frac{\partial W}{\partial \mathbf{Z}} + \frac{T}{T_0}\frac{\partial}{\partial \dot{\mathbf{Z}}}\left\langle\!\left\langle \Phi\left(\frac{T}{T_0}\frac{\Delta \mathbf{F}}{\Delta t}, \frac{T}{T_0}\frac{\Delta \mathbf{Z}}{\Delta t}\right)\right\rangle\!\right\rangle = 0. \tag{21}$$

Consistency with respect to the continuous operator expresses as

$$\lim_{\Delta t \to 0} \frac{\partial}{\partial \dot{\mathbf{Z}}}\left\langle\!\left\langle \Phi\left(\frac{T}{T_0}\frac{\Delta \mathbf{F}}{\Delta t}, \frac{T}{T_0}\frac{\Delta \mathbf{Z}}{\Delta t}\right)\right\rangle\!\right\rangle = \frac{\partial \Phi}{\partial \dot{\mathbf{Z}}}\left(\dot{\mathbf{F}}, \dot{\mathbf{Z}}\right) \tag{22}$$

Hence, provided known external fields $\{\mathbf{F}, T\}$, the internal variables $\mathbf{Z}$ can be computed at each integration point at each discrete time step.

2.2.2. Incremental boundary value problem

Consider now a discrete time increment for the variational initial boundary value problem, whose object is to compute the external fields $\{\mathbf{u}, T\}$ at each time step. An incremental functional $I(\mathbf{u}, T)$ is sought in such a way that it approximates the integral of the functional Φ (14) over the time increment Δt:

$$\begin{aligned} I(\mathbf{u}, T) = &\int_{\Omega_0}\left[\mathcal{W}(\mathbf{F}, T; \mathbf{F}_0, T_0, \mathbf{Z}_0) - \Delta t\left\langle\!\left\langle \chi\left(-\frac{\boldsymbol{\nabla} T}{T}; \mathbf{F}(\tau), T(\tau), \mathbf{Z}(\tau)\right)\right\rangle\!\right\rangle\right] dV \\ + &\int_{\Omega_0}\left[\Delta t\ \rho\ r \log\frac{T}{T_0} - \rho \mathbf{b}\cdot\Delta\mathbf{u}\right] dV - \int_{\partial_t\Omega_0}\bar{\mathbf{t}}\cdot\Delta\mathbf{u}\, da - \int_{\partial_Q\Omega_0}\Delta t\ \bar{Q}\ \log\frac{T}{T_0}\, da \end{aligned} \tag{23}$$

The time discretized balance laws can be obtained from stationary conditions of the incremental functional (23). Thus, the external fields $\{\mathbf{u}, T\}$ can be computed as optimizers of the above functional at each time step

$$\{\mathbf{u}, T\} = \arg\ \underset{\mathbf{u}, T}{\operatorname{stat}}\ I(\mathbf{u}, T) \tag{24}$$

Most of the times, W is convex in $\mathbf{u}$ and concave in T. Therefore, solution fields can be characterized as a saddle point of the incremental functional:

$$\{\mathbf{u}, T\} = \arg\ \inf_{\mathbf{u}}\sup_{T}\ I(\mathbf{u}, T) \tag{25}$$

2.3. Examples of particular media

2.3.1. Purely thermal transient problem

In the case of a purely thermal problem, the free energy and the dissipation potential respectively reduce to:

$$W(T) = -\frac{\rho C}{2}\frac{(T - T_{\text{ref}})^2}{T_{\text{ref}}} \tag{26}$$

and

$$\chi(-\boldsymbol{\nabla} T) = \frac{1}{2T_{\text{ref}}}\boldsymbol{\nabla} T\cdot\mathbf{K}\cdot\boldsymbol{\nabla} T \tag{27}$$

where C is the specific heat capacity, $\mathbf{K}$ the heat conductivity tensor, and T_{ref} some reference temperature. The incremental potential (23) then takes the following form (up to a constant factor T_{ref}):

$$I(T) = \int_\Omega\left\{\frac{C}{2\Delta t}(T_{n+1} - T_n)^2 + \frac{1}{2}\boldsymbol{\nabla} T_{n+1}\cdot\mathbf{K}\cdot\boldsymbol{\nabla} T_{n+1} - r(T_{n+1} - T_n)\right\} dV \tag{28}$$

It is easy to see that the discrete weak form coupled to an implicit Euler finite difference scheme is obtained by taking the first variation of the above functional:

$$< D_T I, \delta T >= \int_\Omega \left\{ \frac{C}{\Delta t}(T_{n+1} - T_n)\delta T + \boldsymbol{\nabla}\delta T \cdot \mathbf{K} \cdot \boldsymbol{\nabla} T_{n+1} - r\delta T \right\} dV = 0 \tag{29}$$

2.3.2. Linear thermo-elasticity

For linear thermo-elasticity in the linearized geometrical framework, Helmholtz's free energy takes the form:

$$W(\boldsymbol{\varepsilon}, T) = \frac{1}{2}\boldsymbol{\varepsilon} : \mathbf{C} : \boldsymbol{\varepsilon} - \boldsymbol{\varepsilon} : \mathbf{C} : \boldsymbol{\alpha}(T - T_{\text{ref}}) - \frac{1}{2}\rho C \frac{(T - T_{\text{ref}})^2}{T_{\text{ref}}} \tag{30}$$

where $\boldsymbol{\varepsilon}$ denotes the linearized strain tensor, $\mathbf{C}$ the elastic stiffness tensor, $\boldsymbol{\alpha}$ the tensor of thermal dilatation, C the specific heat capacity (at constant strain) and T_{ref} the reference temperature. Denoting the temperature increment as $\theta = T - T_{\text{ref}}$, the constitutive law reads:

$$\boldsymbol{\sigma} = \frac{\partial W}{\partial \boldsymbol{\varepsilon}} = \mathbf{C} : (\boldsymbol{\varepsilon} - \boldsymbol{\alpha}\theta) \tag{31}$$

2.3.3. Thermo-elasto-visco-plasticity

For thermo-elasto-visco-plastic media, a multiplicative decomposition is applied to the deformation gradient $\mathbf{F} = \mathbf{F}^e \cdot \mathbf{F}^p$ [40]. In the linearized geometrical framework, the linearized strain $\boldsymbol{\varepsilon}$ is additively split into elastic and plastic part $\boldsymbol{\varepsilon} = \boldsymbol{\varepsilon}^e + \boldsymbol{\varepsilon}^p$. Helmholtz's free energy is defined in this case as:

$$W(\boldsymbol{\varepsilon}, \boldsymbol{\varepsilon}^p, T) = W^e(\boldsymbol{\varepsilon} - \boldsymbol{\varepsilon}^p, T) + W^p(\boldsymbol{\varepsilon}^p, T) + W^t(T) \tag{32}$$

where W^e is the elastically stored energy (recoverable), W^p is the plastically stored energy (not directly recoverable) and W^t the thermally stored energy (heat capacity). The reversible stress $\boldsymbol{\sigma}^{\text{rev}}$ is then given by:

$$\boldsymbol{\sigma}^{\text{rev}} = \frac{\partial W}{\partial \boldsymbol{\varepsilon}} = \frac{\partial W^e}{\partial \boldsymbol{\varepsilon}} = \mathbf{C} : ((\boldsymbol{\varepsilon} - \boldsymbol{\varepsilon}^p) - \boldsymbol{\alpha}\theta) \tag{33}$$

Denoting the back stress by $\mathbf{X} \equiv -\frac{\partial W^p}{\partial \boldsymbol{\varepsilon}^p}$, the mechanical dissipation $\mathscr{D}_{\text{mech}}$ reads

$$\mathscr{D}_{\text{mech}} = -\frac{\partial W}{\partial \boldsymbol{\varepsilon}^p} : \dot{\boldsymbol{\varepsilon}}^p = \left(\frac{\partial W^e}{\partial \boldsymbol{\varepsilon}^e} - \frac{\partial W^p}{\partial \boldsymbol{\varepsilon}^p} \right) : \dot{\boldsymbol{\varepsilon}}^p = (\boldsymbol{\sigma} - \mathbf{X}) : \dot{\boldsymbol{\varepsilon}}^p \geq 0 \tag{34}$$

and should be non-negative. A plastic flow rule corresponding to von Mises-type plasticity can be written as follows:

$$\dot{\boldsymbol{\varepsilon}}^p = \dot{\bar{\varepsilon}}^p \mathbf{M} \tag{35}$$

where $\dot{\bar{\varepsilon}}^p$ stands for some effective plastic strain rate, and $\mathbf{M}$ its flow direction. The dissipation potential $\Phi(\dot{\bar{\varepsilon}}^p; \bar{\varepsilon}^p, T)$ takes the general form:

$$\Phi(\dot{\bar{\varepsilon}}^p; \bar{\varepsilon}^p, T) = \begin{cases} \phi(\dot{\bar{\varepsilon}}^p; \bar{\varepsilon}^p, T) & \text{if } \dot{\bar{\varepsilon}}^p \geq 0 \\ +\infty & \text{otherwise} \end{cases} \tag{36}$$

with ϕ a convex function such that $\phi(0; \bar{\varepsilon}^p, T) = 0$ and $\partial_{\dot{\bar{\varepsilon}}^p} \phi(0; \bar{\varepsilon}^p, T) = \sigma_Y(\bar{\varepsilon}^p, T) \geq 0$, where σ_Y denotes the tensile yield stress. For rate-independent plasticity, ϕ can be considered as:

$$\phi = \sigma_Y \dot{\bar{\varepsilon}}^p \tag{37}$$

More details about the incremental variational formulation of thermo-visco-elasto-plasticity and the implementation of specific models in finite strain can be found in [66] and [65].

3. Variational h-adaption algorithm

3.1. Refinement

3.1.1. Adaption criteria

The incremental variational problem results is an optimization problem of the form:

$$\inf_{\mathbf{u}\in\mathcal{V}} \quad \sup_{T\in\mathcal{W}} \quad I_h(\mathbf{u}, T) \tag{38}$$

where $\mathcal{V}$ and $\mathcal{W}$ refer to spaces of continuous and regular functions defined in the domain Ω_0, respecting Dirichlet boundary conditions. A staggered solution scheme for the coupled problem [1] is preferred, which allows to use different meshes for the mechanical and the thermal parts.

In finite element analysis, the solutions lie in subspaces $\mathcal{V}_h$ and $\mathcal{W}_h$ of $\mathcal{V}$ and $\mathcal{W}$ respectively, which are built from nodal shape functions associated with the triangulations $\mathscr{T}_u$ and $\mathscr{T}_T$ of the domain Ω_0. In the present context of mesh adaption, $\mathcal{V}_h$ and $\mathcal{W}_h$ are the nets of linear spaces generated by edge bisection and parameterized by a directed index set A[1]. Hence, dime($\mathcal{V}_{h1}$) ≤ dime($\mathcal{V}_{h2}$) if the triangulation $\mathscr{T}_{h2}$ corresponding to $\mathcal{V}_{h2}$ can be reached from $\mathscr{T}_{h1}$ by successive edge bisections. The initial triangulation and the solution space corresponding to the initial mesh are $\mathscr{T}_0$ and $\mathcal{V}_0$ respectively. Therefore, the corresponding element $0 \in A$ precedes all the other elements.

For regular problems, the variational functional is convex with respect to the displacement field, and concave with respect to the temperature field. This provides a comparison criterion to judge the quality of meshes. Thus, a triangulation $\mathscr{T}_{u_1}$ associated with a displacement field $\mathbf{u}_1$ can be judged better than a triangulation $\mathscr{T}_{u_2}$ with a displacement field $\mathbf{u}_2$ if and only if $I(\mathbf{u}_1, T) < I(\mathbf{u}_2, T)$. Similarly, a triangulation $\mathscr{T}_{T_1}$ associated with a temperature field T_1 can be judged better than a triangulation $\mathscr{T}_{T_2}$ with a temperature field T_2 if and only if $I(\mathbf{u}, T_1) > I(\mathbf{u}, T_2)$. This allows to formulate the problem of variational mesh adaption as an optimization problem:

$$\inf_{\mathbf{u}\in\mathcal{V}_h} \quad \sup_{T\in\mathcal{W}_h} \left\{ I_h(\mathbf{u}, T) + \mu_g^u N_u - \mu_g^T N_T \right\} \tag{39}$$

where N_u and N_T are the number of nodes of the triangulations of the mechanical and thermal meshes respectively. Indeed, the *global* parameters μ_g^u and μ_g^T are needed to define a criterion to stop the mesh adaption process because additional degrees of freedom will never worsen the variational potential. When a node is added to the mechanical mesh, the value of the potential I_h decreases, while N_u increases by one. The net effect of the addition of one node is an offset by an amount μ_g^u due to the second term in equation (39). *Hence, mesh refinement is only admissible if the node added to the mechanical mesh reduces the potential I_h by a value greater than μ_g^u.* Similarly, when a node is added to the thermal mesh, the value of the potential I_h increases, while N_T increases by one. The net effect of an additional node in the thermal mesh in equation (39) is an offset by an amount μ_g^T due to the third term. For the thermal part, mesh refinement is only admissible if a node added to the thermal mesh increases the potential I_h by a value greater than μ_g^T. Therefore, the parameters μ_g^u and μ_g^T appear as the energetical costs linked to the addition of a new node in the mechanical and the thermal meshes respectively, which should be strictly positive. If the improvement of the value of the incremental functional is more than that of the cost of a node, refinement is admissible.

Assuming the mechanical problem is solved before the thermal one in a staggered approach, the mesh adaption problem (39) can be represented separately for the mechanical and the thermal meshes at a given time step t_n as:

$$\inf_{\mathbf{u}\in\mathcal{V}_h} \left\{ I_h(\mathbf{u}_n, T_{n-1}) + \mu_g^u N_u \right\} \equiv \inf_{\mathbf{u}\in\mathcal{V}_h} \mathcal{I}_u(\mathbf{u}_n, T_{n-1}, N_u) \tag{40}$$

$$\sup_{T\in\mathcal{W}_h} \left\{ I_h(\mathbf{u}_n, T_n) - \mu_g^T N_T \right\} \equiv \sup_{T\in\mathcal{W}_h} \mathcal{I}_T(\mathbf{u}_n, T_n, N_T) \tag{41}$$

However, it is sometimes convenient to solve the thermal problem before the mechanical one, especially when a weak coupling is considered with a one-way effect of the thermal part onto the mechanical part. In such scenario, the mesh

[1] A directed set is a nonempty set A together with a binary relation ≤ with properties of reflexivity($a \le a, \ \forall a \in A$), transitivity(if $a \le b$ and $b \le c$, then $a \le c$), and directedness(for any pair $a, b \in A$, there exists a $c \in A$ such that $a \le c$ and $b \le c$).

adaption problem can be stated as follows:

$$\sup_{T\in\mathcal{W}_h}\left\{I_h(\mathbf{u}_{n-1},T_n)-\mu_g^T N_T\right\}\equiv\sup_{T\in\mathcal{W}_h}\mathcal{I}_T(\mathbf{u}_{n-1},T_n,N_T) \tag{42}$$

$$\inf_{\mathbf{u}\in\mathcal{V}_h}\left\{I_h(\mathbf{u}_n,T_n)+\mu_g^u N_u\right\}\equiv\inf_{\mathbf{u}\in\mathcal{V}_h}\mathcal{I}_u(\mathbf{u}_n,T_n,N_u) \tag{43}$$

In the above expressions, fields with subscript $n-1$ are computed at the previous time step. Equation (40) adapts the mechanical mesh and computes the displacement solution $\mathbf{u}_n$ at time t_n. Equation (41) considers $\mathbf{u}_n$ as given, adapts the thermal mesh and computes the thermal solution T_n at time t_n. The converse operates in equations (42) and (43), for which the mechanical and thermal steps are swapped.

Problems (40)-(41) and (42)-(43) are of combinatorial complexity, that is, for each value of number of nodes, several meshes with different values of incremental variational functional are possible. Thus, infinite choices of number of nodes are possible. This combinatorial complexity makes these problems very hard to solve in general. Hence, a greedy approach is used by means of an iterative procedure in order to take advantage of the additive property of the incremental variational potential, $I_h(\mathbf{u},T)=\sum_i^{nElem} I_i(\mathbf{u}_i,T_i)$. The geometry is divided into patches, and refinable elements are collected from each patch. This is done by locally refining each patch and checking the following condition for the mechanical part:

$$I_i^l(\mathbf{u}_1^l,T^l)-\inf_{\mathbf{u}_2^l\in\mathcal{V}} I_i^l(\mathbf{u}_2^l,T^l)>\mu_{lr}^u\Delta N_u \tag{44}$$

where I_i^l represents the incremental variational potential for the i^{th} patch (l stand for *local*), $\mathbf{u}_1^l$ and $\mathbf{u}_2^l$ refer to the displacement field computed on the original and the refined patch respectively, T^l is the thermal field interpolated from a different thermal mesh, μ_{lr}^u is the cost linked to the addition (r stands for refinement) of a new node in a patch of the mechanical mesh, and ΔN_u denotes the number of new nodes introduced in the refined patch. Similarly, the following condition is verified by the thermal part:

$$\sup_{T_2^l\in\mathcal{W}} I_i^l(\mathbf{u}^l,T_2^l)-I_i^l(\mathbf{u}^l,T_1^l)>\mu_{lr}^T\Delta N_T \tag{45}$$

where T_1^l and T_2^l refer to the temperature fields computed on the original and the refined patch respectively, $\mathbf{u}^l$ is the displacement field interpolated from a different mechanical mesh, μ_{lr}^T is the cost linked to the addition of a new node in the patch of the thermal mesh and ΔN_T is the number of new nodes introduced in the refined patch. If the improvement of the incremental functional due to the introduction of an additional node is greater than the energetical cost associated with the addition of a node in this patch, the refined mesh of the patch is retained, otherwise, the original mesh of the patch is kept. Checking conditions (44) and (45) involves the solution of a local problem on the refined patch with fixed Dirichlet boundary conditions on its boundary (which are available from the previous global solution).

3.1.2. Local adaption techniques

Two methods are considered in this work for the construction and the refinement of patches. The first one is the single edge bisection technique [50]. It consists in identifying a single edge in the mesh to be bisected, from which a patch is identified as the ring of elements around this edge. For $P1$ elements, the refinement process introduces one node, as shown in Figure 1. For a boundary edge, a similar process is applied, as shown in Figure 2. For $P2$ elements, if the target edge is on the boundary, three new nodes are added, otherwise four new nodes are added. No bound is here applied on the element aspect ratio, therefore meshes obtained tend to be anisotropic because the variational approach does not apply any constraint on the geometrical aspect of the mesh. This can provide different degrees of spatial resolution in different directions suitable for the problem under investigation at the cost of elongated elements.

The second one is the longest edge propagation path (LEPP) strategy of Rivara [60, 59], that allows to guarantee an upper bound on the element aspect ratio. The list of edges to be bisected is obtained from the algorithm of Rivara and the patch is constructed by taking the union of elements around these edges. The process is illustrated in Figure 3.

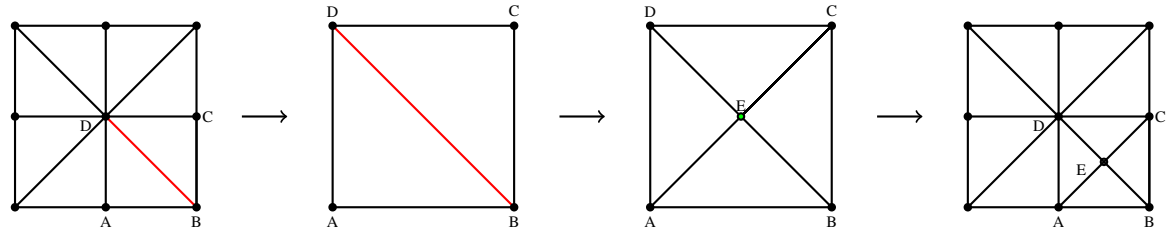

Figure 1: The edge identified is BD. Therefore, the patch contains the two elements adjacent to the edge BD. The refined version of patch contains the new node E. If the edge is on the boundary, the original patch will only have a single element.

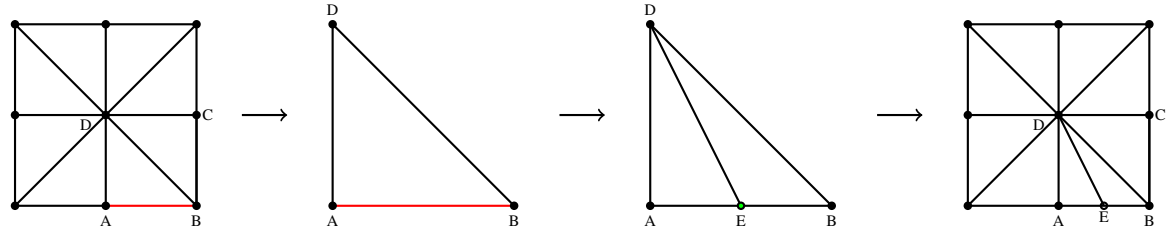

Figure 2: The edge identified is AB, which is on the boundary. Therefore, the patch contains a single element DAB. The refined version of the patch contains the new node E.

3.2. Coarsening

For transient problems, the domains of interest evolve with the time and the loading. Therefore, mesh coarsening is also important to adapt the mesh in such a way that the sole domain of interest be refined. The process of mesh coarsening is similar to that of mesh refinement. The identification of a previously refined edge, candidate for a potential coarsening, allows to go back to the original mesh irrespective of the method of refinement used. For example, consider the refinement obtained by the LEPP strategy as shown in Figure 3. One can easily go back to the original mesh by a two-step coarsening procedure as shown in Figure 4. The following condition associated with coarsening is checked for the mechanical problem on each patch:

$$\inf_{\mathbf{u}_2^l \in \mathcal{V}} I_i^l(\mathbf{u}_2^l, T^l) - I_i^l(\mathbf{u}_1^l, T^l) < \mu_{ld}^u \tag{46}$$

where $\mathbf{u}_1^l$ and $\mathbf{u}_2^l$ refer to the displacement fields computed on the original and coarsened patches respectively, and μ_{ld}^u is the cost associated with the removal (d stands for derefinement) of a node in the i^{th} patch of the mechanical mesh. Note that only one node is removed from the patch, therefore the resulting increase of the incremental potential should be less than the energetical cost associated with a single node. Similarly for a thermal problem, the following condition is checked on each patch:

$$I_i^l(\mathbf{u}, T_1^l) - \sup_{T_2^l \in \mathcal{W}} I_i^l(\mathbf{u}, T_2^l) < \mu_{ld}^T \tag{47}$$

where T_1^l and T_2^l refer to the temperature fields computed on the original and the coarsened patches respectively, and μ_{ld}^T is the cost associated with the removal of a node in the i^{th} patch of the thermal mesh. Here, the decrease of the incremental potential caused by coarsening should be less than the energetical cost associated with a single node. In other words, if the saving of energetical cost associated with a node is greater than the effect on the solution field due to the removal of a node, the patch can be coarsened. Conversely, if the deterioration of the solution due to the removal of a node is significant with respect to the energy cost associated with a node, the patch is not coarsened in order to obtain a sufficiently accurate solution. Note that allowing different values for the parameters μ_{ld}^u, μ_{ld}^T, μ_{lr}^u, μ_{lr}^T, μ_g^u and μ_g^T can give a better control over the adaption procedure.

3.3. Mesh adaption procedure

The mesh adaption procedure including refinement and coarsening steps can be summarized as follows:

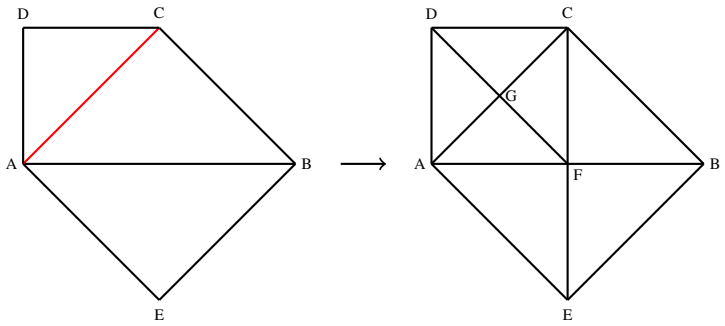

Figure 3: The edge identified is AC, the triangles ACD and ACB share this edge. The segment AC is the longest edge for the triangle ACD but not for the triangle ACB. The longest edge of the triangle ACB is AB. The edge AB is shared by triangles ACB and AEB. Since AB is the longest edge for both of them, it is the terminal longest edge in LEPP and is hence first bisected. Then the edge AC is bisected which is now the terminal longest edge in LEPP. Here, the patch contains three elements and two new nodes, but in general it can contain any number of elements corresponding to the Longest Edge Propagation Path (LEPP).

Algorithm 3.1 (Staggered computation and adaption of meshes).
Provided the solutions $(\mathbf{u}_{n-1}, T_{n-1}, \mathbf{Z}_{n-1})$ *defined on their respective meshes at time* t_{n-1},

1. *Solve the mechanical problem*
   while *convergence is not obtained, iterate on k such that*
   - *(i) Adapt the mechanical mesh by checking conditions* (44) *and* (46) *on each patch.*
   - *(ii) Find* $\mathbf{u}_n^{(k)}$ *by minimizing* (40).
   - *(iii) Update* $\mathbf{Z}_n^{(k)}$ *at each Gauss point of the mechanical mesh by minimizing the local functional* $\mathscr{I}(\mathbf{F}_n^{(k)}, T_{n-1}, \mathbf{Z}_n^{(k)}; \mathbf{F}_{n-1}, \mathbf{Z}_{n-1})$ (20)
2. *Solve the thermal problem*
   while *convergence is not obtained, iterate on k such that*
   - *(i) Adapt the thermal mesh by checking conditions* (45) *and* (47) *on each patch.*
   - *(ii) Find* $T_n^{(k)}$ *by maximizing* (41).
   - *(iii) Update* $\mathbf{Z}_n^{(k)}$ *at each Gauss point of the thermal mesh by minimizing the local functional* $\mathscr{I}(\mathbf{F}_n, T_n^{(k)}, \mathbf{Z}_n^{(k)}; \mathbf{F}_{n-1}, T_{n-1}, \mathbf{Z}_{n-1})$ (20)

If the thermal and mechanical steps are swapped, equations (40)-(41) are replaced by equations (42)-(43). For practical implementation purpose, the above μ parameters that are homogeneous to an energy are replaced by three

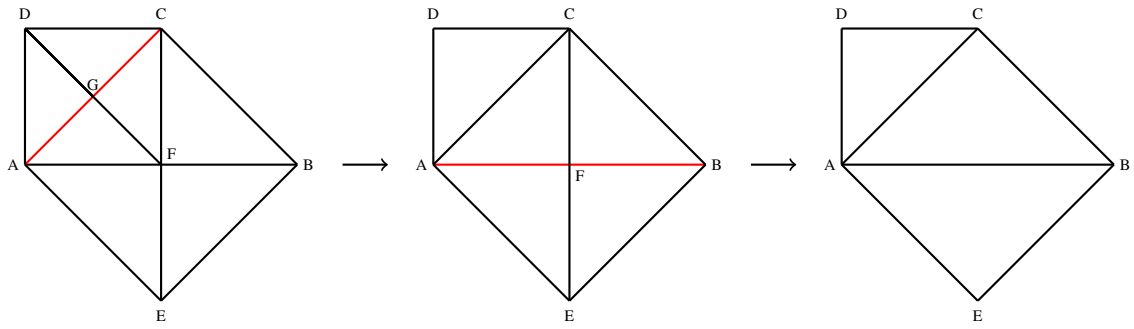

Figure 4: The LEPP algorithm gives the single step refinement of several edges. They are coarsened one by one. Here edge AGC is coarsened to AC first, then edge AFB is coarsened to AB.

dimensionless parameters, namely Tol_r, Tol_d and Tol_0, respectively associated with the refinement of a patch of element, its derefinement, and the global iterative processus on a mesh. These parameters are defined on both thermal and mechanical meshes, so that six parameters can be defined in a thermomechanical analysis. Convergence criteria are defined on some relative improvement of the variational functional between two iterations. More details about this point as well as about the definition and the influence of tolerance parameters can be found in [55], and are hence not repeated here.

3.4. Management of internal variables

Mesh adaption problems often involve complex remapping procedures for transferring the internal variable set from an initial mesh to an adapted mesh. Remapping of internal variables causes significant numerical diffusion. In the present work, the internal variables are assumed to be piece-wise constant over elementary cells consisting of the intersection between Voronoï cells and triangular elements. Therefore, at any given point in an element, the values of internal variables are assumed to be equal to that of the closest integration point within that element as shown in Figure 5.

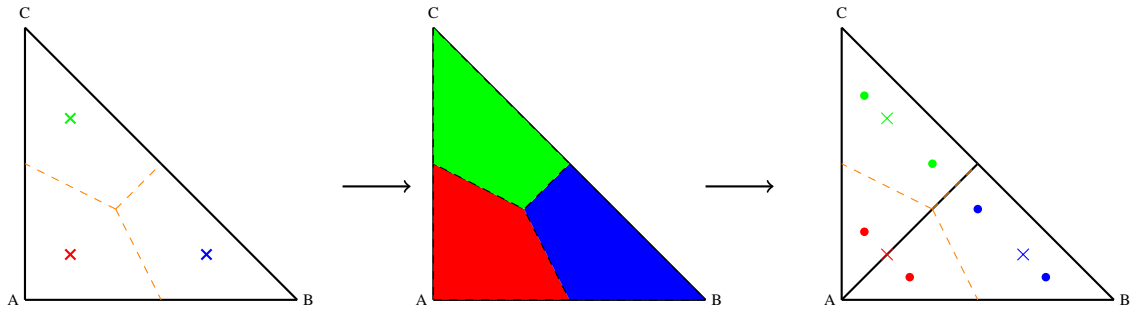

Figure 5: The sketch on the left shows a triangular parent element with three integration points shown in different colours. Pieces of Voronoï cells intersected with that triangle corresponding to each Gauss point are shown in the sketch at the middle. These elementary cells represent the domain of influence of each Gauss point. The right sketch on the right shows the bisected triangle, hence generating two new triangles. The children Gauss points inherit data from parent Gauss points, as shown in the same colors.

Upon edge bisection, when a new integration point is created, the process of remapping involves simple inheritance of internal variables at the new integration point from the closest integration point in the parent element. In this way, children elements remain consistent with the history of deformation of their parent elements and satisfy the internal constraints. Upon coarsening, the integration point inherits internal variables from the closest integration point within the refined elements. Again, parent elements remain consistent with the average history of deformation of their children elements and satisfy the internal constraints. This variational transfer operator is dealt with in detail by Ortiz and Quigley [52].

3.5. Interpolation of fields from one mesh to another

The coupled thermo-mechanical problem is solved with a staggered approach using two different meshes for the mechanical and the thermal parts. In order to deal with the coupling effects, information transfer from one mesh to another is necessary. For nodal fields, this transfer consists of a simple interpolation of fields to the Gauss points of the other mesh. Therefore, given an integration point, a search is made to find the element in the other mesh in which the integration point lies. Using the nodal values, a finite element interpolation is performed. For variables defined at integration points, the process consists in finding the closest integration point in the other mesh and the values are inherited. Using spatial coordinates, a linear search can allow to obtain the element in the other mesh in which the current integration point lies. This process is shown in Figure 6.

Using external fields $\mathbf{u}$ and T obtained by interpolation from their respective meshes to a particular integration point, internal variables are updated using the local variational problem (20), as explained in algorithm 3.1.

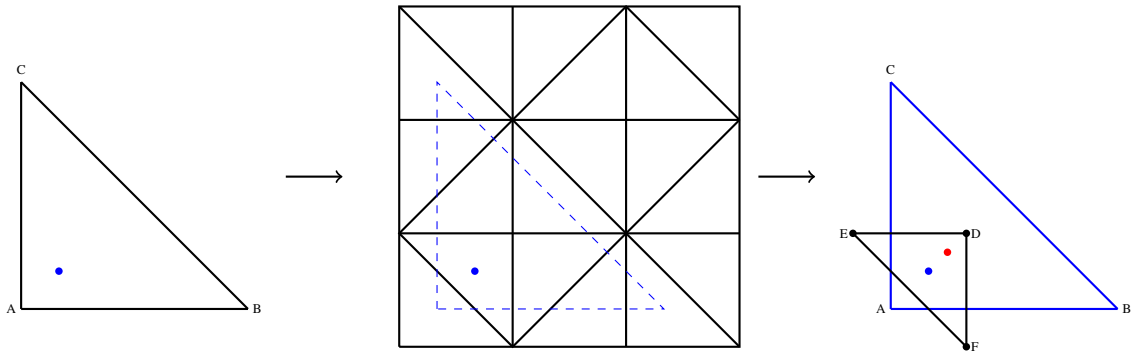

Figure 6: The sketch on the left shows an element ABC and one of its Gauss points, on which fields from the other mesh are to be interpolated. The sketch at the middle shows the other mesh and the element ABC in blue dotted line. The element in which the Gauss point of the element ABC lies is identified as the element DEF as shown in the sketch on the right. Therefore, the external fields can be interpolated from nodal values of nodes D, E and F. The variables at integration points are inherited from the closest integration point in the element DEF, shown in red.

4. Examples

4.1. Steady state thermal problem

The proposed mesh adaption strategy is first tested on a steady state thermal example whose analytical solution is known. Consider a rectangular plate of width W and height H, subjected to the following boundary conditions, summarized in Figure 7:

$$\begin{aligned} T &= T_1 \qquad \text{at } x = 0 \text{ and } x = W \ \forall y \in]0, H[, \ y = 0 \ \forall x \in]0, W[\\ T &= T_2 \qquad \text{at } y = H \ \forall x \in]0, W[\end{aligned} \tag{48}$$

The analytical solution for this test case can be found in [32, Chapter 3], and is given as follows:

$$\frac{T - T_1}{T_2 - T_1} = \frac{2}{\pi} \sum_{n=1}^{\infty} \frac{(-1)^{n+1} + 1}{n} \sin\left(\frac{n\pi x}{W}\right) \frac{\sinh(n\pi y/W)}{\sinh(n\pi H/W)} \tag{49}$$

The prescribed boundary conditions impose a jump of temperature from T_1 to T_2 at the two top corners of the plate (see Figure 7). Because of this jump, the incremental variational functional (23) is expected to indicate a necessary drastic improvement of the solution through refinement of patches close to these two corners, hence leading to a very fine mesh in these areas due to this singularity.

This simulation of mesh adaption was carried out on a square of unit length, starting from a mesh of four 6-node triangular elements as shown in Figure 7, and the edge bisection technique was used for mesh refinement. The refinement parameter Tol_r and the global tolerance parameter Tol_0 are here set to 10^{-4} and 10^{-5} respectively. The final adapted mesh and the solution field are shown in Figure 8. As expected, the obtained adapted mesh is very fine near the two top corners. Note also that the obtained mesh is symmetric with respect to a middle vertical line, and is well structured. This is due to the symmetry of the geometry and of the loading of this problem. The algorithm can also be combined with other patching strategies to produce meshes with desired geometric characteristics.

Next, the efficiency of the algorithm is analyzed by computing the L_2 error between the numerical and analytical temperatures, as a function of the number of nodes of the mesh. Three cases are considered. First, a plot is made for some uniform meshes, and will be used as a reference. A comparison of the variational mesh adaption with respect to the $ZZ2$ Superconvergent Patch Recovery method [73, 74] was already performed in [55] leading to quite comparable results, and is hence not repeated here. Second, the L_2 error is plotted at each refinement iteration of the adaptive mesh algorithm with respect to the current number of nodes of the mesh. However, since the mesh adaption is done in several iterations, a consistent comparison between a uniform and the variational refinement should account for the path of refinement followed during the mesh adaption procedure. One way to achieve this is to account for a cumulated number of nodes associated with all the computations performed during the mesh adaption process. Therefore, a third

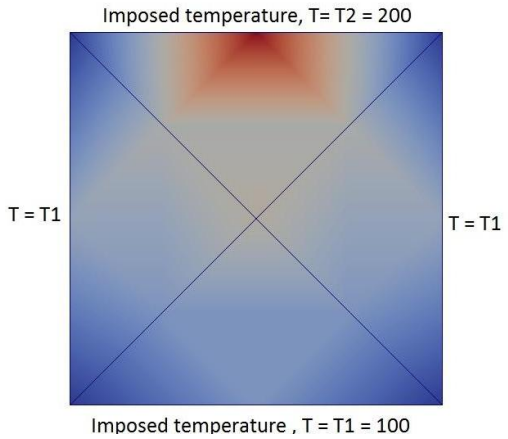

Figure 7: Solution field on the initial mesh along with the boundary conditions.

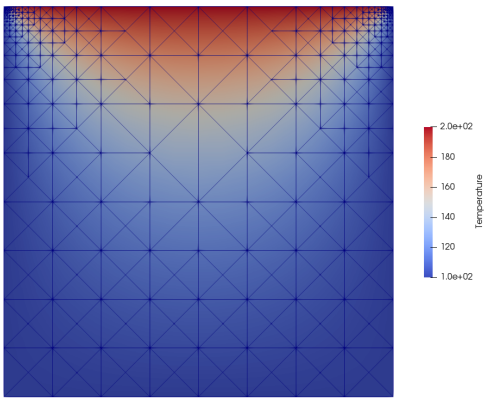

Figure 8: Numerical solution on the adapted mesh.

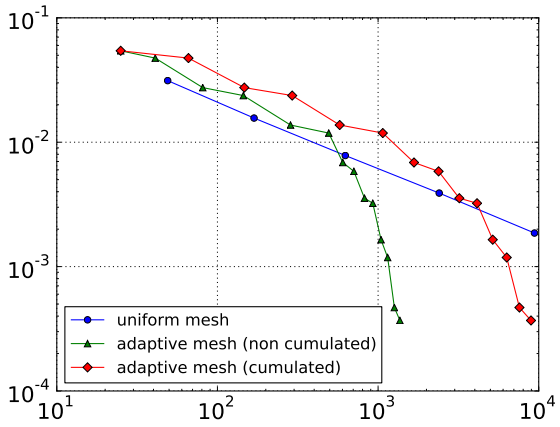

Figure 9: Analysis of the algorithm. Number of nodes on X axis and L_2 error in temperature on Y axis.

plot consists of the error computed at each refinement iteration of the variational adaptive mesh algorithm with respect to the cumulated number of nodes.

Figure 9 shows these superposed plots. It can be observed that the plot linked to the cumulated number of nodes crosses the uniform one from above, meaning that a more precise solution can be obtained with less computational cost using variational mesh adaption.

4.2. Linear thermo-elastic holed plate

Consider a rectangular plate with a circular hole, made of a linear thermoelastic material. The plate is submitted to compression through a negative prescribed normal displacement on its top face, in the Y direction. Making use of the symmetries, only one quarter of the plate is modelled. A zero heat flux boundary condition is prescribed for the thermal part on the whole boundary, whereas for the mechanical part symmetry conditions are accounted for at planes $x = 0$ and $y = 0$ in addition to the prescribed negative displacement. Figure 10 shows the computational domain and the boundary conditions, and Table 1 lists the numerical values of data associated with the geometry, the loading and the material parameters. The loading is applied linearly on the time interval $t \in [0, 1]$ s.

The purpose of this test case is to compare the single edge bisection [50] and Rivara's [60, 59] mesh adaption techniques. Also, this test case shows an application of the variational mesh adaption algorithm to a strongly coupled

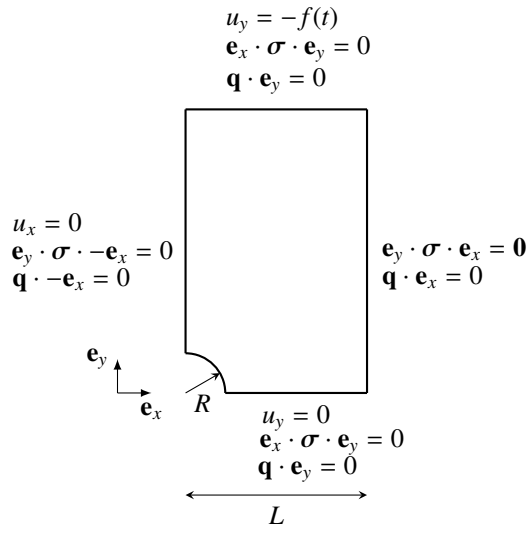

Figure 10: Geometry and boundary conditions for the thermo-elastic problem.

Geometry	
L	32×10^{-3} m
H	50×10^{-3} m
R	2.5×10^{-3} m
Loading	
$\dot{f}(t)$	10^{-4} m.s^{-1}
Material parameters	
ρ	1450 kg.m^{-3}
E	2×10^{9} Pa
ν	0.35
α	6×10^{-5} K^{-1}
T_{ref}	300 K
C	148 J.kg^{-1}.K^{-1}
k	1×10^{-2} W.m^{-1}.K^{-1}

Table 1: Numerical data

Mechanical mesh	
Tol_0	10^{-3}
Tol_r	10^{-4}
Tol_d	10^{-4}
Thermal mesh	
Tol_0	0.1
Tol_r	0.1
Tol_d	0.1

Table 2: Tolerance parameters for the holed plate

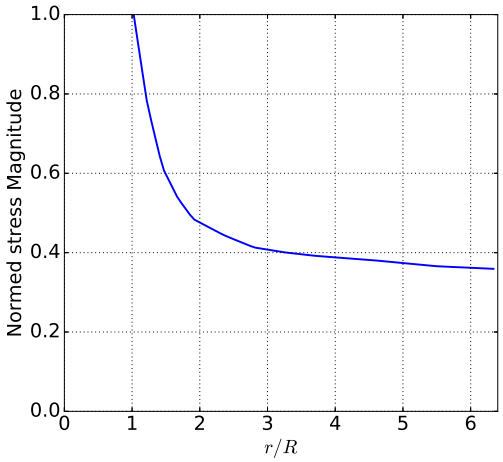

(a) Stress magnitude

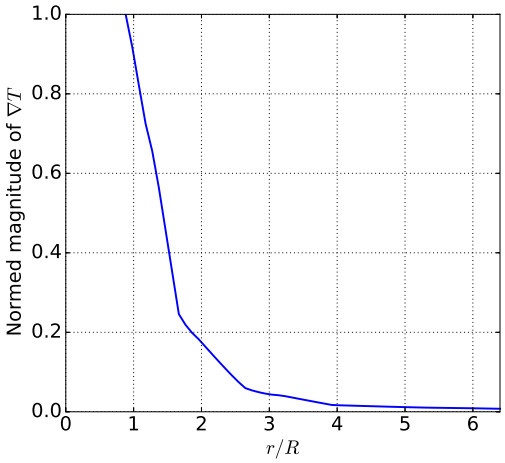

(b) Magnitude of the temperature gradient

Figure 11: Plots along the ligament ($y = 0$).

problem, applying an isothermal staggered scheme [1] with P1 finite elements.

Figure 11 shows some plots of the solution along the ligament ($y = 0$), obtained with an initial coarse mesh. Due to the stress concentration near the hole as shown in Figure 11(a), the mechanical mesh adaption should produce a finer mesh around the hole at the first time step. The same holds for the thermal one, because of high temperature gradients in that area, as shown in Figure 11(b). Unlike the purely transient thermal test [55], severe mesh coarsening and refinement should not be observed at each time step here, because the domain of interest does not change with respect to time.

Provided the tolerance parameters listed in Table 2, Figures 12(a) and 12(b) show the adapted meshes for the mechanical part obtained by using simple patches consisting of two triangles, and by using Rivara's patch respectively. Observe that in both cases, a fine mesh has been generated close to the hole, and a coarser one is let far from it.

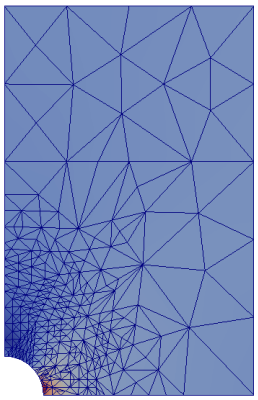

(a) Adapted mechanical mesh consisting of 329 nodes obtained using the single edge bisection technique.

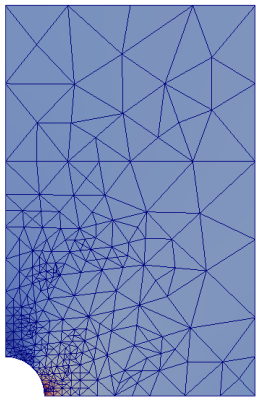

(b) Adapted mechanical mesh consisting of 340 nodes obtained using Rivara's technique.

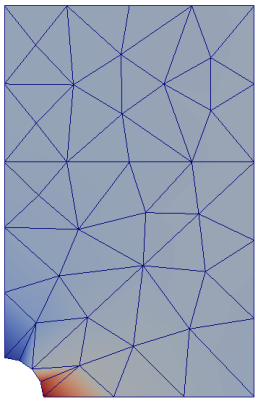

(c) Adapted thermal mesh consisting of 44 nodes obtained using the single edge bisection technique.

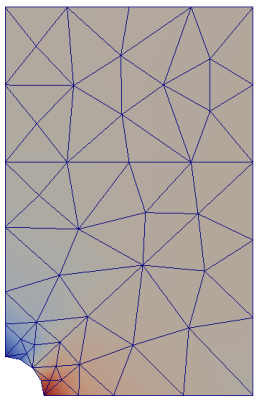

(d) Adapted thermal mesh consisting of 53 nodes obtained using Rivara's technique.

Figure 12: Adapted meshes

Therefore, these two meshes allow to represent a good solution field. However, it is observed in Figure 12(a) that the mesh has elongated elements, and has become anisotropic. This difference is even more evident on the temperature field shown in Figures 12(c) and 12(d). Observe the four elongated elements in Figure 12(c). This anisotropy is avoided in Rivara's algorithm by finding the LEPP (Longest Edge Propagation Path) and refining backwards as shown in Figure 12(d). It is important to note that the mesh adaption is performed only at the first time step and no major changes in the mesh are observed after the first time step.

In order to compare the edge bisection and Rivara's mesh adaption techniques, the mesh adaption process is allowed to continue for a few more iterations at the first time step. For comparison purpose, the parameters for both cases are chosen such that the precision level of the solution is of similar order of magnitude. We here leverage the fact that the mesh adaption is only performed at the first time step. Figures 13 and 14 show the comparison of the potential energy computed for the mechanical and the thermal mesh respectively. It can be observed that the edge bisection converges towards slightly better values of the potential energy for both thermal and mechanical meshes. Indeed, since Rivara's technique directly applies a constraint on the element aspect ratio and hence yields a constrained optimization problem, it is normal to find slightly less optimal values of the potential energy than these obtained with the edge bisection, which is associated with an unconstrained optimization problem. In the latter, the sole underlying

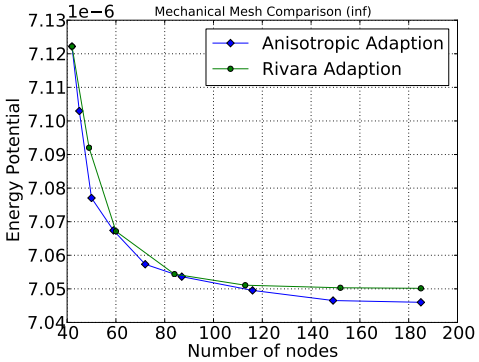

Figure 13: Comparison of mesh adaption techniques for the mechanical mesh.

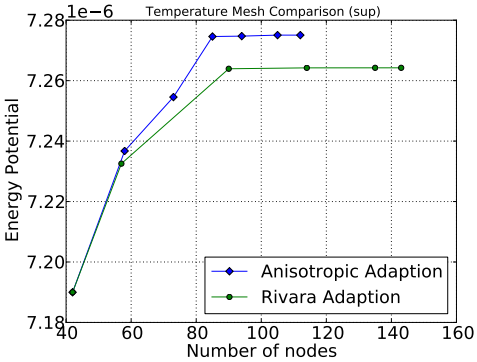

Figure 14: Comparison of mesh adaption techniques for the thermal mesh.

physics drives the mesh adaption through the value of the potential energy, and may hence show this small difference.

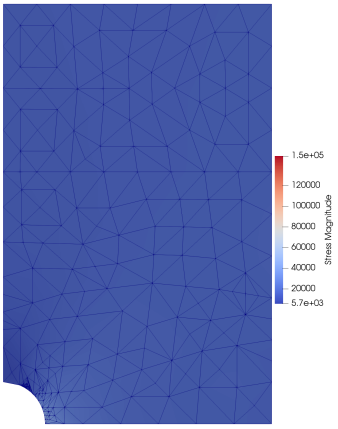

(a) Adapted mechanical mesh at early stages.

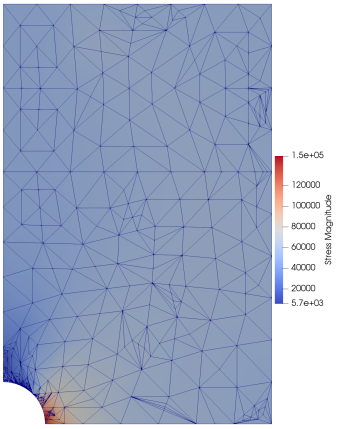

(b) Adapted mechanical mesh at final time.

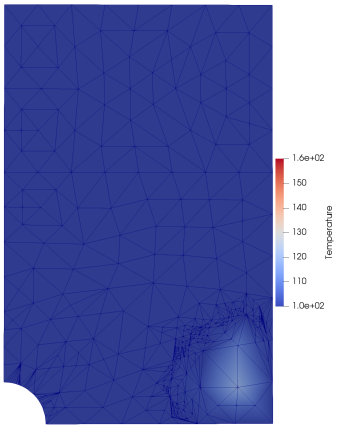

(c) Adapted thermal mesh at early stages.

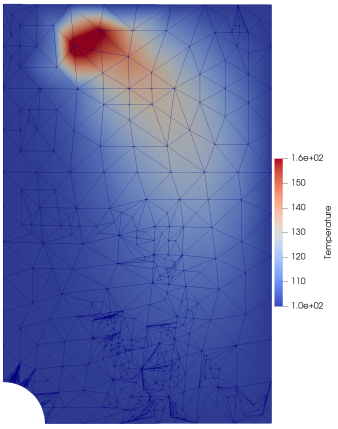

(d) Adapted thermal mesh at final time.

Figure 15: Adapted meshes with a prescribed moving heat source

The holed plate is now submitted to a heat source, moving along an elliptical path about the hole center of the thermoelastic plate. The heat source has a magnitude of 10^5W.m^{-3}, a width of 10^{-3}m and an angular range of 2°, while the ellipse has semi-major and semi-minor axes set at 15.5×10^{-3} and 24.5×10^{-3}m respectively.

Figure 15 shows the mechanical and thermal meshes at early stages and at final time of the simulation. When the heat source is suddenly applied, the thermal mesh is refined around it to capture the strong thermal gradients (see Figure 15(c)), while the mechanical mesh does not show nor need such refinement in the same area (see Figure 15(a)). As the heat source moves along its elliptical path, derefinement has occured because the temperature distribution has been smoothed with time (Figure 15(d)). Meanwhile, the mechanical mesh has continued to be refined close to the hole as the compression loading has increased with time (Figure 15(b)).

4.3. Shear banding

A shear band is a narrow region experiencing an instability due to thermal softening associated with large deformation, high strain rate and high temperature rise, occurring in various ductile materials [67]. The well-known hat shaped specimen [47] has been designed to trigger such shear banding in dynamical testing in order to study the shear response of some metallic alloys undergoing large strains, high strain rate and high temperature.

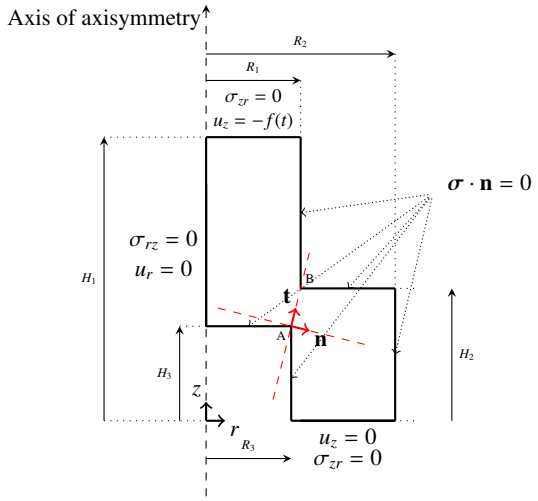

Figure 16: Geometry and mechanical boundary conditions of shear band specimen.

Geometry	
H_1	15×10^{-3} m
H_2	7×10^{-3} m
H_3	5×10^{-3} m
R_1	5×10^{-3} m
R_2	10^{-2} m
R_3	4.5×10^{-3} m

Table 3: Numerical data for the hat shaped specimen

Mechanical mesh	
Tol_0	0.1
Tol_r	10^{-2}
Tol_d	0.1
Thermal mesh	
Tol_0	0.3
Tol_r	0.9
Tol_d	0.9

Table 4: Tolerance parameters for the shear banding test case

The present test case serves to show the good performance of the variational mesh adaption for complex coupled problems in the framework of finite strains. However, some simplifications are considered here: the loading is not prescribed as fast as it is in the experimental test and inertia terms are neglected. The thermo-elastic-viscoplastic constitutive model developed in [66] is used for the hat shaped specimen, with the materials parameters associated with an α-Titanium alloy which is known to be strain rate dependent. In particular, this constitutive model accounts for isotropic strain-hardening and thermal softening. The geometry and the boundary conditions of the axisymmetric hat shaped specimen are shown in Figure 16, and associated numerical values are listed in Table 3. A zero heat flux is imposed on the whole boundary, and the specimen is compressed by means of a normal displacement of 5×10^{-5} m prescribed on the top face of the specimen, linearly on the time interval $t \in [0, 5]$ s. The geometry and the imposed displacement cause high shear stresses distributed along the segment AB, supported by the unit vector $\mathbf{t}$ shown in Figure 16. Next, the mechanical dissipation causes a rise of temperature along the direction $\mathbf{t}$, leading to the softening of the material. Softening causes an increase of plastic strains such that a narrow shear band appears.

For the simulation, the same initial mesh is used for both mechanical and thermal parts, as shown in Figure 17. Rivara's LEPP mesh adaption technique is used in the presented results. An isothermal splitting is used along with P1 finite elements, and the values used for the tolerance parameters are listed in Table 4. The final adapted thermal mesh at the final time step is shown along with its temperature distribution in Figure 18. Mesh adaption can be seen in areas where a sharp temperature gradient needs to be captured. Similarly, the final adapted mechanical mesh at the final

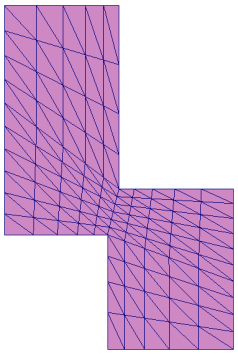

Figure 17: Initial mesh for both thermal and mechanical parts.

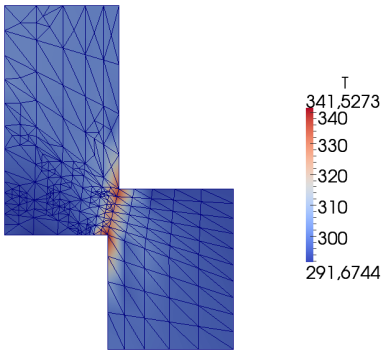

Figure 18: Final adapted thermal mesh with temperature isovalues.

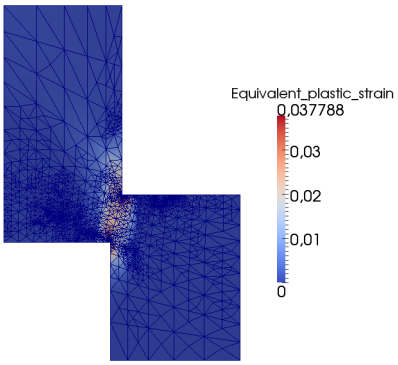

Figure 19: Final adapted mechanical mesh with equivalent plastic strain isovalues.

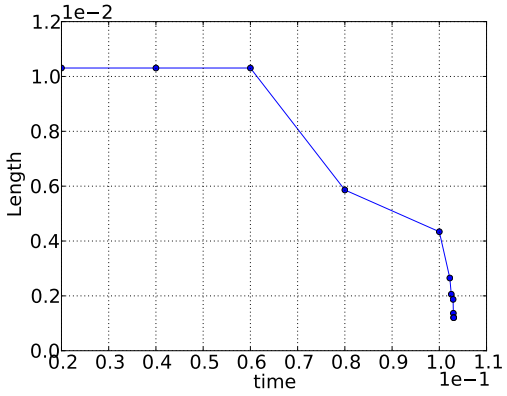

Figure 20: Evolution in time of the length of the segment computed with $k = 0.3$ in equation (50).

time step along with the field of equivalent plastic strain is shown in Figure 19. Zooms on areas close to the sheared zone are shown in Figures 21 and 22.

Estimating the width of the shear band is known to be a real challenge with standard isothermal finite element analyses, since the modeling used may not include any internal length. However, thermal conduction solved here allows to introduce such an internal length into the modeling [41, 16, 25], and hence allows to regularize the problem by avoiding the width of the shear band to converge to an element length as the mesh is refined.In order to analyze the evolution of the temperature increase in the narrow band with time, the length of a segment l, normal to the shear band, is plotted along the direction $\mathbf{n}$ (see Figure 16). More precisely, the segment l is defined as:

$$l = \{x \mid T(x) > kT_{max}\}, 0 < k < 1. \tag{50}$$

It corresponds to a certain width linked to the stencil of sharp temperature rise due to the appearance of the shear band. At the beginning, a quite uniform temperature over the domain leads the segment l to cover its whole length in the direction $\mathbf{n}$. As soon as the shear band appears, the temperature increases in the band, causing the length of the segment l to drop. This evolution is shown in Figure 20. The decrease of the length with time is the image of some increase of the temperature. The time evolution of the average shear stress σ_{nt} along the segment AB ($(\mathbf{n}, \mathbf{t})$ being shown in Figure 16) is shown in Figure 23. It is observed that the shear stress increases until time 0.10 seconds. Next, the material softening starts, an evident temperature rise occurs, whose maximum value is shown in Figure 24, which causes a decrease of the shear stress. A kink appearing in the temperature profile can be clearly observed at time 0.10

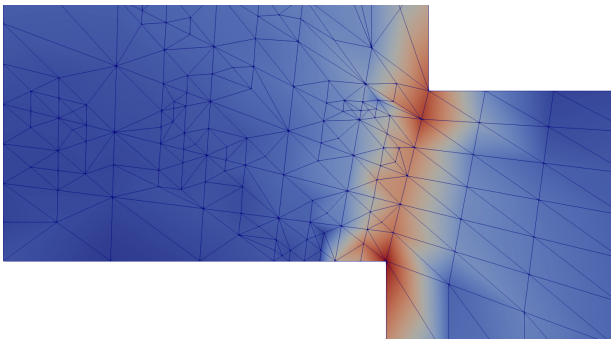

Figure 21: Zoom on the final adapted thermal mesh with temperature isovalues.

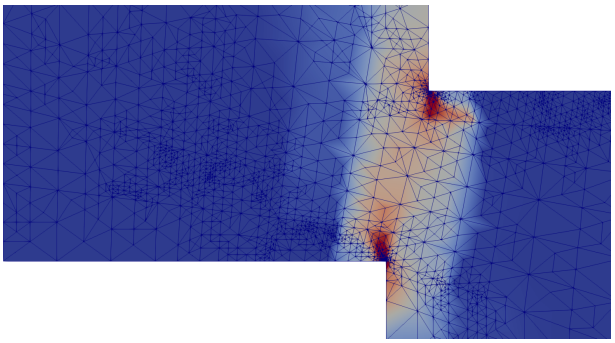

Figure 22: Zoom on the final adapted mechanical mesh with equivalent plastic strain isovalues.

seconds.

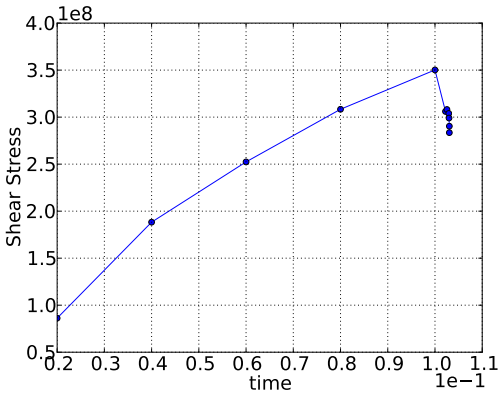

Figure 23: Evolution of $\langle \sigma_{nt} \rangle_{AB}$ with time.

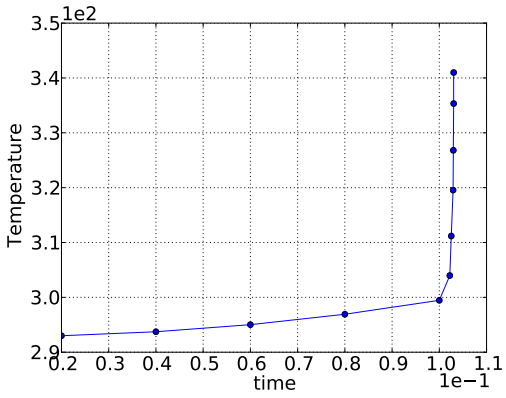

Figure 24: Evolution of maximum temperature T_{max} with time.

Su et al. [67] used an analytical solution developed by Leroy et al. [41] for a 1D shear band problem. The temperature distribution predicted in the band is given by:

$$T(y) = T_{max} - (T_{max} - T_{ref}) \frac{\log\left(\cosh\left(\frac{y}{h}\right)\right)}{\log\left(\cosh\left(\frac{H}{h}\right)\right)}, \tag{51}$$

and the velocity is given by

$$V(y) = V_0 \frac{\tanh\left(\frac{y}{h}\right)}{\tanh\left(\frac{H}{h}\right)}. \tag{52}$$

However, this solution is valid for a 1D problem with prescribed temperature boundary conditions and a specific constitutive model. Therefore, a regression is used in order to find the parameter h appearing in equations (51) and (52). That model also neglects the elastic part of the strain so that plastic strains are compatible with the displacement field. The analytical expression of the plastic strain rate is then obtained by taking the gradient of the velocity V (52). The plots shown in Figures 25 and 26 show the numerical and analytical solutions of the temperature and the plastic strain rate along the direction $\mathbf{n}$, neglecting the domains close to boundaries. It can be seen that the analytical and numerical profiles are close. The differences are essentially due to the different boundary conditions. This test case shows how accurate solutions of complex strongly coupled problems can be obtained using the proposed mesh adaption strategy.

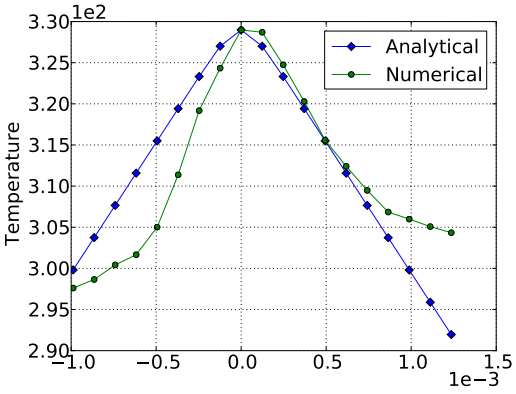

Figure 25: Numerical and analytical temperature profile along $\mathbf{n}$ at time 1.03×10^{-2} seconds.

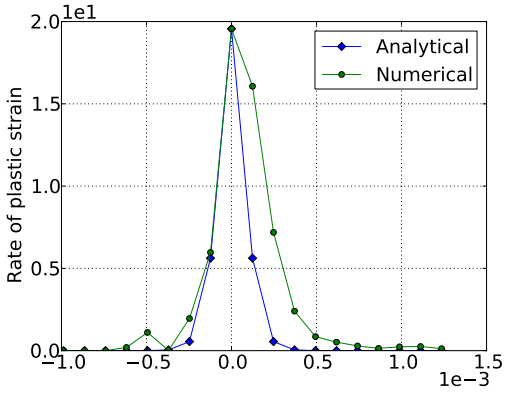

Figure 26: Numerical and analytical rate of plastic strain along $\mathbf{n}$ at time 1.03×10^{-2} seconds.

4.4. Linear friction welding

Linear friction welding is an industrial process in which the two parts to be welded are put in contact with a given pressure, then rubbed against each other. The friction causes a rise of temperature, which leads to the softening of materials up to that they get welded.

Since this process involves a very strong thermo-mechanical coupling, this is an interesting test case to show the good behavior of the proposed variational mesh adaption technique. Numerical simulation of linear friction welding has already been studied, among others, by Debeugny [20], Foca [23] who used a mesh free approch for simulating the process, but also by Li *et* al. [42] who used a complete remeshing to advance the simulation. However, the latter procedure may cost loss in precision due to significant numerical diffusion. Figure 27 shows the geometry and the

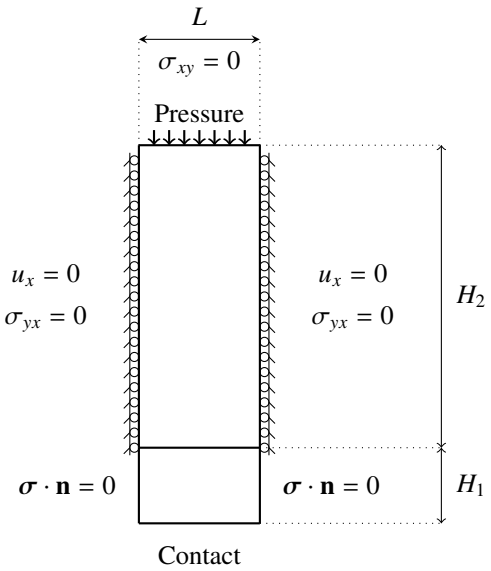

Figure 27: Geometry and boundary conditions of the linear friction welding problem, extracted from [42].

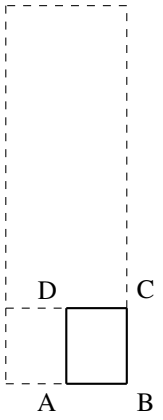

Figure 28: Simplified modeling of the problem. Symmetry boundary condition is applied on AD, contact and heat flux on AB, free tractions on BC and imposed displacement on DC.

Geometry	
L	17×10^{-3} m
H_1	10^{-2} m
H_2	30×10^{-3} m

Table 5: Numerical data for the linear friction welding test case.

Mechanical mesh	
Tol_0	10^{-2}
Tol_r	5×10^{-3}
Tol_d	5×10^{-3}
Thermal mesh	
Tol_0	0.1
Tol_r	0.5
Tol_d	0.5

Table 6: Tolerance parameters for the linear friction welding test case

boundary conditions used by Li *et* al. [42]. In order to focus on effects generated by the linear friction welding, the sole bottom part of the specimen is considered, with free lateral boundary conditions, as shown in Figure 28 with

numerical values listed in Table 5. Next, half of this bottom part is meshed due to symmetry, so that $u_x = 0$ and $\mathbf{q} \cdot \mathbf{n} = 0$ are applied on the segment AD. This modelling assumes that the area above the line DC shown in Figure 27 is rigid, hence the loading is prescribed by means of a displacement u_y imposed on that segment. Contact is applied on the segment AB for the mechanical part, and a given heat flux is prescribed in order to model the heat generation due to friction. The applied heat flux can be assessed as follows, assuming that all the heat generated during friction contributes to the input heat flux $\bar{q}$:

$$\bar{q} = \boldsymbol{\tau} \cdot \mathbf{v} = 4\tau\alpha f \tag{53}$$

where $\mathbf{v}$ denotes the tangential velocity, α the magnitude of the sliding motion imposed between the two parts to be welded, f the frequency of oscillations and τ the shear stress whose magnitude can be evaluated by Coulomb's law:

$$\tau = \mu\sigma_N \tag{54}$$

where μ is the friction coefficient and σ_N is the normal stress. Parameters used for the loading and Coulomb's law are extracted from Li *et* al. [42]. At last, the part to be welded is assumed to be made of Ti-6Al-4V alloy, whose constitutive response of the medium is modelled by the thermo-elasto-visco-plastic Johnson-Cook model [35]. The numerical implementation of the latter in the variational framework and the values of material parameters associated with Ti-6Al-4V can be found in [67].

(a) Thermal initial mesh

(b) Mechanical initial mesh

Figure 29: Initial meshes

The initial meshes used for the thermal and mechanical parts are shown in Figure 29. The single edge bisection technique is used for the mesh adaption in this problem. At the beginning of the loading, high strains occur close to the boundary, causing some refinement of the mechanical mesh in that region as shown in Figure 30. After a few time steps, the mesh is adapted according to the stress field as shown in Figure 31. Figure 32 shows the stress field at the final computed time step.

At the beginning, the adapted thermal mesh easily captures the smooth temperature field, as shown in Figure 33. The maximum temperature is reached close to the contact surface, while it is almost uniform far from it. This causes a finer mesh to develop between these two zones in order to capture the temperature gradient. The adapted thermal mesh along with the associated temperature isovalues are shown in Figure 34 at the final computed time step. A finer refinement appears close to the contact boundaries because of the mechanical effects seen in Figure 32. Figures 35 and 36 show time evolutions of the temperature and the stress magnitude at a point located at the middle of the bottom line. It can be seen that these time evolutions are smooth, the temperature keeping on increasing while the stress magnitude tend to reach a plateau.

The proposed variational mesh adaption strategy thus appears useful for test cases involving strong thermo-mechanical coupling along with large deformations.

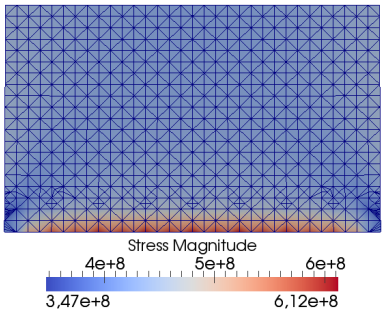

Figure 30: Magnitude (Frobenius norm) of the stress field shown on the deformed mechanical mesh (The solution has been mirrored for display) at preliminary stages.

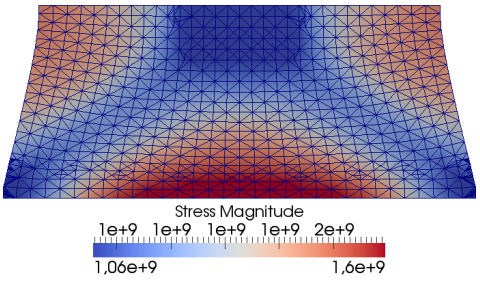

Figure 31: Magnitude (Frobenius norm) of the stress field shown on the deformed mechanical mesh (The solution has been mirrored for display) after developed stress field.

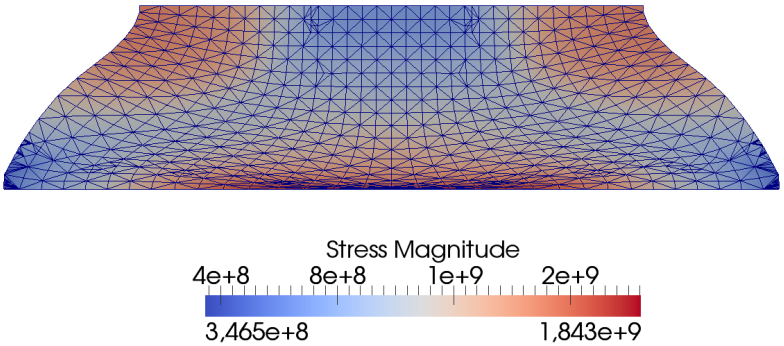

Figure 32: Magnitude (Frobenius norm) of the stress field shown on the deformed mechanical mesh (The solution has been mirrored for display) at the last computed time step.

5. Conclusion

A mesh adaption strategy for coupled thermo-mechanical problems based on a variational approach was presented in this work. The adaption criteria are based on a multifield variational principle, whose discrete incremental functional plays the role of an error indicator. The approach is hence free from error estimates and associated computational cost. The solution procedure uses a staggered scheme, which is leveraged to associate different meshes to the different physics in presence in order to capture their respective different scales and spatial resolutions.

Complex remapping procedures and excessive numerical diffusion is avoided by using a simple interpolation for nodal fields and the closest integration point for fields defined at Gauss points. Indeed, since mesh refinement leads to nested successive meshes, diffusion is controlled. The single edge bisection as well as Rivara's mesh adaption techniques have been used and compared on different test cases. The proposed approach shows good performance on strongly coupled problems and industrial-like processes, like shear banding and linear friction welding. As a perspective, the method could be readily extended to three-dimensional problems. The basic simple edge bissection

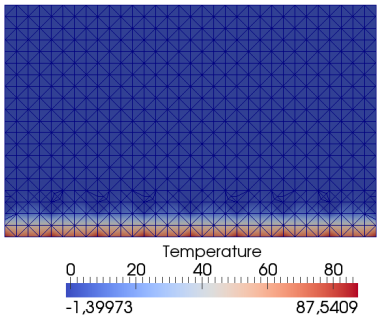

Figure 33: Temperature field shown on the undeformed thermal mesh (The solution has been mirrored for display) at preliminary stages.

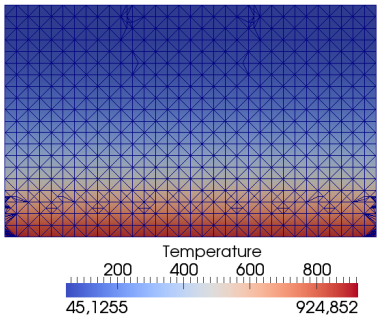

Figure 34: Temperature field shown on the undeformed thermal mesh (The solution has been mirrored for display) at the final time step.

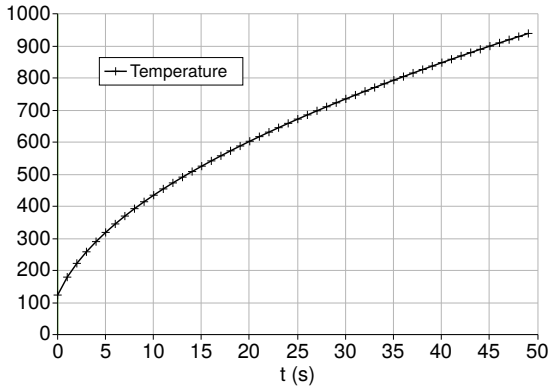

Figure 35: Time evolution of the temperature of the middle bottom point.

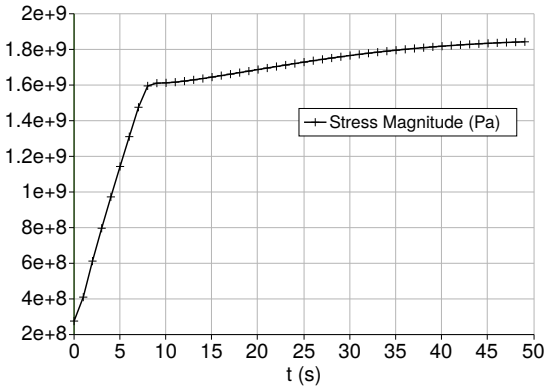

Figure 36: Time evolution of the stress magnitude (Frobenius norm) of the middle bottom point.

can certainly be used in 3D problems. Besides, the extension to the 3D case of LEPP-bisection algorithm is discussed in [61].

Funding

Rohit Pethe was funded by Ecole Centrale de Nantes through Doctoral School SPIGA (ED 498).

References

[1] Armero, F., Simo, J., 1992. A new unconditionally stable fractional step method for non-linear coupled thermomechanical problems. International Journal for Numerical Methods in Engineering 35, 737–766.
[2] Babuska, I., Szabo, B., 1982. On the rate of convergence of finite element method. International journal of numerical methods in engineering 18, 323–341.
[3] Balzani, D., Ortiz, M., 2012. Relaxed incremental variational formulation for damage at large strains with application to fiber-reinforced materials and materials with truss-like microstructures. International Journal for Numerical Methods in Engineering 92, 551–570.
[4] Bathe, K., Zhang, H., 2009. A mesh adaptivity procedure for CFD and fluid-structure interactions. Computers and Structures 87, 604–617.
[5] Batra, G., 1989. On a principle of virtual work for thermo-elastic bodies. Journal of Elasticity 21, 131–146.
[6] Batra, R., Ko, K., 1992. An adaptive mesh refinement technique for the analysis of shear bands in plane strain compression of a thermovis-coplastic solid. Computational mechanics 10, 369–379.
[7] Ben-Amoz, M., 1965. On a variational theorem in coupled thermoelasticity. Journal of Applied Mechanics 32, 943–945.
[8] Biot, M., 1956. Thermoelasticity and irreversible thermodynamics. Journal of Statistical Physics 27, 250–253.

[9] Biot, M., 1958. Linear thermodynamics and the mechanics of solids. Proceedings of the third US National Congress of Applied Mechanics , 1–18.
[10] Borouchaki, H., Laug, P., Cherouat, A., Saanouni, K., 2005. Adaptive remeshing in large plastic strain with damage. International journal of numerical methods in engineering 63, 1–36.
[11] Brancherie, D., Villon, P., Ibrahimbegovic, A., 2008. On a consistent field transfer in non linear inelastic analysis and ultimate load computation. Computational Mechanics 42, 213–226.
[12] Brassart, L., Stainier, L., Doghri, I., Delannay, L., 2012. Homogenization of elasto-(visco) plastic composites based on an incremental variational principle. International Journal of Plasticity 36, 86–112.
[13] Camacho, G., Ortiz, M., 1997. Adaptive lagrangian modeling of ballistic penetration of metallic targets. Computer Methods in Applied Mechanics and Engineering 142, 269–301.
[14] Cao, W., Gonzalez, R., Russell, R., 2003. Variational mesh adaptation methods for axisymmetrical problems. SIAM Journal on Numerical Analysis 41, 235–257.
[15] Carini, A., 1996. Colonnetti's minimum principle extension to generally non-linear materials. International Journal of Solids and Structures 33(1), 121–144.
[16] Clifton, R., Molinari, A., 1983. Localisation de la déformation viscoplastique en cisaillement simple: résultats exacts en théorie non linéaire. Comptes rendus de l'Académie des Sciences , 1–4.
[17] Combe, J., Ladevèze, P., Pelle, J., 2002. Discretization error estimation for transient dynamic simulation. Advances in Engineering Software 33, 553–563.
[18] Comi, C., Corigliano, A., Maier, G., 1991. Extremum properties of finite-step solutions in elasto-plasticity with nonlinear hardening. International Journal of Solids and Structures 27(8), 965–981.
[19] Costa, J., Alves, M., 2003. Layout optimization with h-adaptivity of structures. International journal of numerical methods in engineering 58, 83–102.
[20] Debeugny, L., 2013. Contribution à la modélisation et à la compréhension du procédé de soudage par friction linéaire. Ph.D. thesis. Ecole Centrale de Nantes.
[21] Diez, P., Huerta, A., 1999. A unified approach to remeshing strategies for finite element h-adaptivity. Computer Methods in Applied Mechanics and Engineering 176, 215–229.
[22] Erhart, T., Wall, W., Ramm, E., 2006. Robust adaptive remeshing strategy for large deformation transient impact simulations. International journal of numerical methods in engineering 65, 2139–2166.
[23] Foca, M., 2015. On a Local Maximum Entropy interpolation approach for simulation of coupled thermo-mechanical problems. Application to the Rotary Frictional Welding process. Ph.D. thesis. Ecole Centrale de Nantes.
[24] Francfort, G.A., Marigo, J.J., 1998. Revisiting brittle fracture as an energy minimization problem. Journal of the Mechanics and Physics of Solids 46, 1319–1342.
[25] Gioia, G., Ortiz, M., 1996. The two-dimensional structure of dynamic boundary layers and shear bands in thermoviscoplastic solids. Journal of the Mechanics and Physics of Solids 44, 251–292.
[26] Grätsch, T., Bathe, K., 2005. A posteriori error estimation techniques in practical finite element analysis. Computers and Structures 83, 235–265.
[27] Grinspun, E., Krysl, P., Schröder, P., 2002. Charms: A simple framework for adaptive simulation. ACM Trans. Graph. 21, 281–290. URL: http://doi.acm.org/10.1145/566654.566578, doi:10.1145/566654.566578.
[28] Gurtin, M., 2000. Configurational forces as basic concepts of continuum physics. Springer, New York .
[29] Hackl, K., 1997. Generalized standard media and variational principles in classical and finite strain elastoplasticity. Journal of the Mechanics and Physics of Solids 45(5), 667–688.
[30] Han, W., Jensen, S., Reddy, B.D., 1997. Numerical approximations of problems in plasticity: Error analysis and solution algorithms. Numerical Linear Algebra with Applications 4, 191–204.
[31] Herrmann, G., 1963. On variational principles in thermoelasticity and heat conduction. Quarterly of Applied Mathematics 22, 151–155.
[32] Holman, J., 1996. Heat Transfer. McGraw-Hill Companies.
[33] Huang, W., 2001. Variational mesh adaptation: isotropy and equidistribution. Journal of computational physics 174, 903–924.
[34] Huang, W., Sun, W., 2003. Variational mesh adaptation ii: error estimates and monitor functions. Journal of computational physics 184, 619–648.
[35] Johnson, G.R., Cook, W., 1983. A constitutive model and data for materials subjected to large strains, high strain rates, and high temperatures. Proc. 7th Inf. Sympo. Ballistics , 541–547.
[36] Kelly, D., Gago, J., Zienkiewicz, O., Babuska, I., 1983. A posteriori error analysis and adaptive processes in the finite element method. International journal of numerical methods in engineering 19, 1593–1619.
[37] Kintzel, O., Mosler, J., 2011. An incremental minimization principle suitable for the analysis of low cycle fatigue in metals: A coupled ductile-brittle damage model. Computer Methods in Applied Mechanics and Engineering 200, 3127–3138.
[38] Ladevèze, P., Möes, N., 1997. A new a posteriori error estimation for nonlinear time-dependant finite element analysis. Computational Methods for Applied Mechanical Engineering 157, 45–68.
[39] Ladevèze, P., Pelle, J., 2004. Mastering calculations in linear and nonlinear mechanics. Springer, Mechanical Engineering Series .
[40] Lee, E.H., 1969. Elastic-plastic deformation at finite strains. Journal of applied mechanics 36, 1–6.
[41] Leroy, Y., Molinari, A., 1992. Stability of steady states in shear zones. Journal of the Mechanics and Physics of Solids 40, 181–212.
[42] Li, W., Ma, T., Li, J., 2010. Numerical simulation of linear friction welding of titanium alloy: Effects of processing parameters. Materials and Design 31, 1497–1507.
[43] Li, X., Wiberg, N., 1994. A postprocessed error estimate and an adaptive procedure for the semi-discrete finite element in dynamic analysis. International journal of numerical methods in engineering 37, 3585–3603.
[44] Li, Y., Lai, W., Shen, Y., 2019. Variational h-adaption method for the phase field approach to fracture. International Journal of Fracture 217, 83–103.

[45] Martin, J., Kaunda, M., Isted, R., 1996. Internal variable formulations of elastic-plastic dynamic problems. International Journal of Impact Engineering 18(7-8), 849–858.
[46] Marusich, T., Ortiz, M., 1995. Modelling and simulation of high speed machining. International journal of numerical methods in engineering 38, 3675–3694.
[47] Meyer, L., Manwaring, S., 1985. Critical adiabatic shear strength of low alloyed steel under compressive loading, in: International Conference on Metallurgical Applications of Shock-Wave and High-Strain-Rate Phenomena(EXPLOMET85), pp. 657–674.
[48] Molinari, A., Ortiz, M., 1987. Global viscoelastic behavior of heterogeneous thermoelastic materials. International Journal of Solids and Structures 23(9), 1285–1300.
[49] Molinari, J., Ortiz, M., 2002. Three-dimensional adaptive meshing by subdivision and edge-collapsing in finite-deformation dynamic-plasticity problems with application to adiabatic shear banding. International journal of numerical methods in engineering 53, 1101–1126.
[50] Mosler, J., Ortiz, M., 2007. Variational h-adaptation in finite deformation elasticity and plasticity. International Journal of Numerical Methods in Engineering 72, 505–523.
[51] Mosler, J., Ortiz, M., 2009. An error-estimate-free and remapping-free variational mesh refinement and coarsening method for dissipative solids at finite strains. International Journal of Numerical Methods in Engineering 77, 437–450.
[52] Ortiz, M., Quigley, J., 1991. Adaptive mesh refinement in strain localization problems. Computer Method in Applied Mechanics and Engineering 90, 781–804.
[53] Ortiz, M., Stainier, L., 1999. The variational formulation of viscoplastic constitutive updates. Computational Methods for Applied Mechanical Engineering 171, 419–444.
[54] Papadrakakis, M., Babilis, G., Braouzi, P., 1997. Efficiency of refinement procedures for the p-version of the adaptive finite element method. Engineering Computations 14, 98–118.
[55] Pethe, R., Heuzé, T., Stainier, L., 2019. Variational h-adaption for coupled thermo-mechanical problems. Engineering Computations doi:10.1108/EC-05-2019-0243.
[56] Pijaudier-Cabot, G., Bodé, L., Huerta, A., 1995. Arbitrary eulerian lagrangian finite element analysis of strain localization in transient problems. International journal of numerical methods in engineering 38, 4171–4191.
[57] Radovitzky, R., Ortiz, M., 1999. Error estimation and adaptive meshing in strongly nonlinear dynamic problems. Computer Methods in Applied Mechanics and Engineering 172, 419–444.
[58] Rivara, M., 1991. Local modification of meshes for adaptive and/or multigrid finite-element methods. Journal of Computational and Applied Mathematics 36, 79–89.
[59] Rivara, M., 1997. New longest edge algorithm for the refinement and/or improvement of unstructured triangulations. International Journal for Numerical Methods in Engineering 40, 3313–3324.
[60] Rivara, M., Inostroza, P., 1997. Using longest-side bisection techniques for the automatic refinement of delaunay triangulations. International Journal for Numerical Methods in Engineering 40, 581–597.
[61] Rivara, M.C., 2009. Lepp-bisection algorithms, applications and mathematical properties. Applied Numerical Mathematics 59, 2218–2235.
[62] Romero, I., Lacoma, L., 2006. A methodology for the formulation of error estimators for time integration in linear solid and structural dynamics. International journal of numerical methods in engineering 66, 635–660.
[63] Solin, P., Cerveny, J., Dubcova, L., Andrs, D., 2010. Monolithic discretization of linear thermoelasticity problems via adaptive multimesh hp-FEM. Journal of Computational and Applied Mathematics 234, 2350–2357.
[64] Stainier, L., 2011. Consistent incremental approximation of dissipation pseudo-potentials in the variational formulation of thermo-mechanical constitutive updates. Mechanics Research Communications 38(4), 315–319.
[65] Stainier, L., 2013. A variational approach to modeling coupled thermo-mechanical nonlinear dissipative behaviors, in: Advances in Applied Mechanics. Elsevier. volume 46, pp. 69–126.
[66] Stainier, L., Ortiz, M., 2010. Study and validation of a variational theory of thermo-mechanical coupling in finite visco-plasticity. International Journal of Solids and Structures 47, 705–715.
[67] Su, S., Stainier, L., 2015. Energy-based variational modeling of adiabatic shear bands structure evolution. Mechanics of Materials 80, 219–233.
[68] Thoutireddy, P., Ortiz, M., 2004. A variational r-adaptation and shape-optimization method for finite-deformation elasticity. International journal of numerical methods in engineering 61, 1–21.
[69] Vokas, C., Kasper, M., 2010. Adaptation in coupled problems. The international journal for computation and mathematics in electrical and electronic engineering 29, 1626–1641.
[70] Yang, Q., Stainier, L., Ortiz, M., 2006. A variational formulation of the coupled thermo-mechanical boundary-value problem for general dissipative solids. Journal of the Mechanics and Physics of Solids 54, 401–424.
[71] Ziegler, H., 1977. An introduction to thermomechanics. Elsevier/North-Holland.
[72] Zienkiewicz, O., Zhu, J., 1987. A simple error estimator and adaptive procedure for practical engineering analysis. International journal of numerical methods in engineering 24, 337–357.
[73] Zienkiewicz, O.C., Zhu, J.Z., 1992a. The superconvergent patch recovery and a posteriori error estimates. part 1: The recovery technique. International Journal for Numerical Methods in Engineering 33, 1331–1364.
[74] Zienkiewicz, O.C., Zhu, J.Z., 1992b. The superconvergent patch recovery and a posteriori error estimates. part 2: Error estimates and adaptivity. International Journal for Numerical Methods in Engineering 33, 1365–1382.